Materials Advances

ROYAL SOCIETY OF CHEMISTRY

PAPER

View Article Online
View Journal | View Issue

Cite this: *Mater. Adv.*, 2025, 6, 2029

Pioneering wound care solutions: triaxial wet-spun fibers with bioactive agents for chronic wounds, part II (controlled release and biological activity of the active agents)†

Catarina S. Miranda,[a] A. Francisca G. Silva,[b] Camille Evenou,[c] Jérôme Lamartine,[c] Berengere Fromy,[c] Sílvia M. M. A. Pereira-Lima,[b] Artur Ribeiro,[de] Susana P. G. Costa,[b] Natália C. Homem[f] and Helena P. Felgueiras *[a]

The incidence of bacterial infections associated with chronic wounds (CWs) has increased in recent years. Thus, a triaxial wet-spun fibrous system (containing three layers) was produced for CW healing. The triaxial fibers were loaded with cinnamon leaf oil (CLO), endowed with high antibacterial, antioxidant and anti-inflammatory features, and an antimicrobial peptide –alanine–alanine–proline–valine (AAPV) – capable of regulating the activity of human neutrophil elastase (HNE; highly expressed during inflammatory processes). To overcome the characteristic high volatility of essential oils (EOs), CLO was loaded at the system's core and blended with polycaprolactone (PCL) which has excellent elasticity and tensile strength. The intermediate layer was composed of sodium alginate (SA) which has high hydration capacity and AAPV. Finally, the shell was made of cellulose acetate (CA), ensuring the system's structural integrity and providing a porous network for the controlled release of AAPV and CLO. This research was divided into two parts, with the present addressing the biological characterization of the system, namely the controlled release of bioactive agents, their antibacterial, antioxidant and cytocompatibility profiles and the peptide-loaded fiber ability to inhibit HNE activity. AAPV-loaded wet-spun fibers attained a sustained release of up to 55% during 24 h of incubation in physiological-like media, also presenting effective HNE inhibition (≈65%). Additionally, CLO-loaded fibers demonstrated a controlled release of up to ≈52% during 24 h of incubation in PBS, reaching higher antibacterial and antioxidant profiles in comparison with the unloaded fibers. Data confirmed the biological potential, safety and suitability of the proposed system for future applications in CW care.

Received 5th November 2024,
Accepted 14th February 2025

DOI: 10.1039/d4ma01104j

rsc.li/materials-advances

1. Introduction

Chronic wounds (CWs) cannot heal at the same pace as acute wounds.[1] CWs often stall at inflammation, conditioning the patients' health and their quality of life, leading to chronic pain, loss of function and mobility, and ultimately raising morbidity rates.[2] Frequently, these wounds are the result of bacterial infections, triggered by *Staphylococcus aureus*, *Staphylococcus epidermidis*, *Escherichia coli* and *Pseudomonas aeruginosa*, some of the most prevalent microorganisms and a major concern for the World Health Organization.[2,3] Between 2005 and 2022, *P. aeruginosa* was detected in 14.5% of CWs in the United States of America (USA), while in the United Kingdom (UK) and Portugal, its presence was detected in 8.6% and 11.4% of the cases, respectively.[4] Moreover, in CWs, neutrophils release proteases (including human neutrophil elastase, HNE) in an uncontrolled manner, as soon as bacteria start colonizing the wound site. Such abnormally high concentrations of HNE

[a] *Centre for Textile Science and Technology (2C2T), University of Minho, Campus of Azurém, 4800-058 Guimarães, Portugal. E-mail: catarina.miranda@2c2t.uminho.pt, helena.felgueiras@2c2t.uminho.pt; Fax: +351-253-510-293; Tel: +351-253-510-283*
[b] *Centre of Chemistry (CQ), University of Minho, Campus of Gualtar, 4710-057 Braga, Portugal. E-mail: id10809@alunos.uminho.pt, silviap@quimica.uminho.pt, spc@quimica.uminho.pt*
[c] *Équipe Intégrité fonctionnelle du tissu cutané (SKIN), Laboratoire de biologie tissulaire et d'ingénierie thérapeutique (LBTI), CNRS UMR5305, Université Lyon I, 7 passage du Vercors, 69367 Lyon Cedex 07, France. E-mail: camille.evenou@ibcp.fr, jerome.lamartine@ibcp.fr, berengere.fromy@cnrs.fr*
[d] *CEB – Centre of Biological Engineering, University of Minho, Braga, 4710-057, Portugal. E-mail: arturibeiro@ceb.uminho.pt*
[e] *LABBELS – Associate Laboratory, Braga, Guimarães, Portugal*
[f] *Simoldes Plastics S.A., Rua Comendador António da Silva Rodrigues, 165, 3720-193, Oliveira de Azeméis, Portugal. E-mail: natalia.homem@simoldes.com*

† Electronic supplementary information (ESI) available. See DOI: https://doi.org/10.1039/d4ma01104j

during inflammatory processes lead to the degradation of endogenous and supplemental growth hormones, which prevent the wounds from progressing to the following steps of the healing process.[1,5,6]

The inhibitory effect of the alanine–alanine–proline–valine (AAPV) tetrapeptide against HNE has been proven to be effective.[6,7] The mechanism of action of the AAPV peptide is not yet fully understood. Still, according to Toth *et al.*, the peptide fits the P-P1 subsites of HNE, resulting in competitive inhibition of HNE activity.[6,8] As for other small peptides, AAPV cannot be used freely in CW therapies due to its low stability in physiological media, as well as high sensitivity to changes in environmental conditions. Also, these peptides present toxicity when used at high concentrations during systemic delivery.[9,10] To prevent such events, these bioactive agents can be incorporated into polymeric structures that offer protection against environmental changes and allow their controlled and localized release, working as an alternative for the use of antibiotics.[7]

Antibiotics are a common tool in the treatment of bacterial infections in CWs.[10,11] However, their excessive use has resulted in the need to think of alternate solutions, including essential oils (EOs), therapeutic agents of natural origin that are mainly composed of mixtures of volatile and lipophilic compounds extracted from several parts of plants.[9,11] EOs contain hydrophobic elements responsible for their inherent analgesic, anti-inflammatory, antioxidant and antibacterial properties.[12,13] The antibacterial effects of EOs result from their ability to disrupt processes related to ion or solute transport, due to their lipophilicity, which facilitate their penetration through the bacterial membrane and the interference with intracellular components.[9,11,14] Cinnamon leaf oil (CLO) is extracted from cinnamon barks and leaves and is mainly formed from eugenol and cinnamaldehyde, which endows the EO with antibacterial abilities.[12,15] The antioxidant and antibacterial properties of eugenol have been extensively addressed.[9,16,17] Additionally, this compound has been reported to possess anti-inflammatory properties, by suppressing the expression of the cyclooxygenase II enzyme.[18] However, similarly to small peptides, the use of EOs in therapeutic approaches comes with limitations, including cytotoxicity at high concentrations, high volatility and sensitivity to external factors, such as temperature, light and oxygen.[9,13] Still, in recent years, research has been disclosed on the loading of EOs and therapeutic peptides onto polymeric fibers that increase these bioactive agent's physiological stability, while preserving their chemical features.[9,19]

Producing polymeric fibrous structures loaded with EOs and/or peptides can be accomplished using spinning techniques, including wet-spinning.[20,21] Wet-spun fibrous constructs display a wide range of diameters and morphologies, along with high porosity. Such properties are favored in biomedicine by enabling cell penetration, adhesion and proliferation, and by resembling physiological microenvironments.[20,22] The goal of the current research was to engineer a triaxial system with bacterial and enzyme-related inhibitory features for promoting wound healing. For that, a wet-spinning approach was carried out to produce fibers with three layers, also known as a triaxial system: (1) a core (innermost layer) made of polycaprolactone (PCL), intended to offer the fibers high elasticity, loaded with CLO to inhibit the growth of both Gram-positive and Gram-negative bacteria;[7,23,24] (2) an intermediate layer made of a blend of sodium alginate (SA) and AAPV, to maintain a moist environment and to regulate the local enzymatic activity, respectively;[6,7] and (3) a shell (outermost layer) composed of cellulose acetate (CA) that ensures structural integrity of fibers and offers protection to the inner layers containing the bioactive compounds.[25] The porosity inherent to the shell allowed a somewhat controlled access to the active agents present in the intermediate layer and the core, releasing AAPV and CLO in a sustained manner.

Research was divided in two parts: part I (under peer revision), chemical, physical, mechanical and thermal characterization of the triaxial system, along with a proof of concept consisting of the production of a small dressing; and part II (present manuscript), biological characterization of the triaxial system. The minimum bactericidal concentration (MBC) and minimum inhibitory concentration (MIC) of CLO, in its free form, were examined against *S. aureus*, *S. epidermidis*, *E. coli* and *P. aeruginosa*. HNE inhibition evaluations were performed to determine the AAPV's maximum inhibitory concentration (IC_M), also in its free form. Additionally, bioactive agent release kinetics studies, from within the fiber systems, were carried out. The HNE inhibition capacity of the engineered fibers was evaluated, as well as their antibacterial and antioxidant properties. Finally, the safety of the triaxial fibers towards skin cell models were investigated *in vitro*. Recently, this technique has drawn attention as a promising tool for developing drug delivery systems for biomedical purposes. However, to the authors' knowledge, there are no reports on the production of Eos and peptide-loaded triaxial wet-spun fibers for wound healing applications.

2. Materials and methods

2.1. Materials

CA (M_n 50.000), PCL (M_n 80.000), SA (from brown algae, medium viscosity), 1,1-diphenyl-2-picrylhydrazyl (DPPH), ethyl cyanoglyoxylate-2-oxime (Oxyma), 1,3-diisopropylcarbodiimide (DIC), dichloromethane (DCM), chloroacetic acid, deuterium oxide (D_2O), elastase from human leukocytes, trypsin inhibitor from soybean, *N*-methoxysuccinyl-Ala-Ala-Pro-Val-*p*-nitroanilide (N-MeO-Suc-Ala-Ala-Pro-Val-*p*-NA), Dulbecco's Phosphate Buffered Saline (DPBS), trypsin–EDTA, Tryptan Blue solution and fetal bovine serum (FBS) were obtained from Sigma-Aldrich (St Louis, Missouri, USA). Antibiotic–antimycotic was obtained from Grisp (Porto, Portugal). *N*,*N*-dimethylformamide (DMF), acetic acid (AcOH), acetonitrile (ACN), piperidine, sodium hydroxide, sodium carbonate, 2,2,2-trifluoroethanol (TFE) and trifluoroacetic acid (TFA) were acquired from Merck (Darmstadt, Germany). Dimethyl sulfoxide (DMSO) and 6-hydroxy-2,5,7,8-tetramethylchroman-2-carboxylic acid (Trolox) were

obtained from Fisher (Maharashtra, India). Dulbecco's Modified Eagle's Medium (DMEM), penicillin–streptomycin, Alamar Blue and lactate dehydrogenase (LDH) kit were purchased from Invitrogen (Massachusetts, USA). Triton was acquired from Bio-Rad Laboratories (California, USA). Anhydrous calcium chloride was employed as coagulation/crosslinking agent during wet-spinning and was supplied by Chem-Lab (Zedelgem, Belgium). Tris–hydrochloride (Tris–HCl) was purchased from Roche (Basel, Switzerland).

AAPV and WAAPV were synthesized by us as described in ref. 7. Pure cinnamon leaf oil (CLO, origin *Cinnamomum zeylanicum* Blume, ρ = 1.049) was obtained from Folha *d*'Água Company (Santo Tirso, Portugal).[19] Sodium phosphate dibasic (Sigma-Aldrich), monosodium phosphate monohydrate (Merck), potassium chloride (Merck) and sodium chloride (Merck) were used in the preparation of phosphate buffer saline solution (PBS at 0.01 M: 1.44 g L^{-1} of Na_2HPO_4, 0.24 g L^{-1} of KH_2PO_4, 0.20 g L^{-1} KCl and 8.00 g L^{-1} of NaCl, adjusted to physiological pH 7.4).

Gram-positive bacteria *S. aureus* (ATCC 6538) and *S. epidermidis* (ATCC 35984), along with Gram-negative bacteria *E. coli* (ATCC 25922) and *P. aeruginosa* (ATCC 25853) were supplied by American Type Culture Collection (ATCC, Virginia, USA). For bacteria growth, trypticase soy broth (TSB), trypticase soy agar (TSA), nutrient agar (NA) and nutrient broth (NB) were purchased from VWR (Alfragide, Portugal), while the Mueller Hinton broth (MHB) was obtained from CondaLab (Madrid, Spain). Human keratinocytes cell line (HaCaT) – DKFZ HaCaT adherent cell line (immortalized human keratinocytes) – was obtained from Cytion (previously known as CLS) (Eppelheim, Germany), and provided by DKFZ (Helmtoz, Germany).[26] Mouse embryonic fibroblast cell line (NIH 3T3) from Sigma Aldrich (Darmstadt, Germany). All reagents were used without further purification.

2.2. Wet-spun fiber production

A PCL solution was prepared in DMF at 10% w/v and stirred for 1 h at 50 °C. CLO was then combined at 16.40 mg mL^{-1} (amount established in ref. 27), consisting of 4× its MIC. Both compounds were left to homogenize for 1 h at 50 °C (PCL–CLO solution).[28] A 2% w/v aqueous SA solution was also prepared and stirred for 3 h at 50 °C. Afterwards, AAPV was added to the previous solution at 50 μg mL^{-1}, corresponding to its maximum inhibitory concentration (IC_M) (concentration established in ref. 7) (SA–AAPV solution). Finally, a 10% w/v CA solution was dissolved in DMF for 3 h at 50 °C. A wet-spinning setup was used, containing three syringe pumps (NE-300, New Era Pump Systems, Norleq, Santo Tirso, Portugal), responsible for controlling the rate and ejection volume, a triaxial spinneret (sealed needles of three layers with 21, 15 and 11 gauge, from the inner to the outer layer) and a large tray containing 500 mL of a 2% w/v $CaCl_2$ coagulation bath, at room temperature (RT). PCL or PCL–CLO solutions were loaded onto the syringe connected to the innermost port (core) and ejected at 0.11 mL min^{-1}, whereas SA or SA–AAPV solutions were loaded onto the intermediate port and ejected at 0.13 mL min^{-1}. Additionally, CA solution was ejected at 0.15 mL min^{-1} and loaded onto the outermost port (shell). Fibers containing only one layer (PCL, PCL–CLO, SA, SA–AAPV, CA) were also produced, as well as fibers without one of the layers (*e.g.*, PCL/SA, PCL/CA, SA/CA). To each group of fibers, samples without one/both of the active agents were also produced in order to test the influence of each compound on the properties of the system (*e.g.*, PCL/SA–AAPV, PCL–CLO/SA/CA). The identification of the fibers used "/" for separating elements belonging to different layers and "–" for components within the same layer (Table 1).

2.3. WAAPV and CLO release kinetics

The monitoring of AAPV release by using IV-visible absorption spectroscopy was not possible, since an overlapping of maximum wavelengths of absorption between all fiber compounds (all biodegradable polymers) was observed. Due to the absence of fluorescence from AAPV, a modified version of the peptide was synthesized, by including the fluorescent amino acid tryptophan (WAAPV), used to monitor the release by fluorimetry. Although the presence of such amino acid may have led to differences in the peptide release rates, such modification still

Table 1 List of wet-spun fiber typologies analyzed in this research

Fiber typology	Core composition	Intermediate layer composition	Shell composition
PCL	PCL	—	—
PCL–CLO	PCL blended with CLO	—	—
SA	—	SA	—
SA–AAPV	—	SA blended with AAPV	—
CA	—	—	CA
PCL/SA	PCL	SA	—
PCL–CLO/SA	PCL blended with CLO	SA	—
PCL/SA–AAPV	PCL	SA blended with AAPV	—
PCL–CLO/SA–AAPV	PCL blended with CLO	SA blended with AAPV	—
SA/CA	—	SA	CA
SA–AAPV/CA	—	SA blended with AAPV	CA
PCL/CA	PCL	—	CA
PCL–CLO/CA	PCL blended with CLO	—	CA
PCL/SA/CA	PCL	SA	CA
PCL–CLO/SA/CA	PCL blended with CLO	SA	CA
PCL/SA–AAPV/CA	PCL	SA blended with AAPV	CA
PCL–CLO/SA–AAPV/CA	PCL blended with CLO	SA blended with AAPV	CA

allowed the prediction of the peptide's behavior in physiological media, due to their similar chemical structures. The fluorescent peptide was loaded onto the fibers as described in ref. 7. A WAAPV calibration curve in PBS at concentrations ranging from 0.500 and 62.500 μg mL^{-1} was prepared using a spectrometer Sarspec (Vila Nova de Gaia, Portugal) and LightScan 2.0 software. WAAPV-loaded fibers were immersed in PBS, pH 7.4, for 1, 2, 4, 6 and 24 h of incubation at 37 °C and 120 rpm, and aliquots of 150 μL were collected at each time point. Fluorescence was then read using an LED lamp of 275 nm, in the range 180–900 nm, with a resolution of 1 nm and wavelength accuracy of ±0.5 nm. Results were reported as intensity counts (IC) *vs.* wavelength, based on the WAAPV calibration curve (IC = 32.413 × Concentration + 4144.7; R^2 = 0.9858).

Regarding the EO, the amount of CLO released from all wet-spun fibers were estimated using a UV-1800 UV-visible spectrophotometer (Shimadzu) (measurement of remaining concentration after fiber immersion). Initially, a calibration curve of CLO at different concentrations in PBS, ranging from 0.02 to 0.20 mg mL^{-1}, was prepared to enable reliable detection of the spectra's region of interest. The results were plotted as absorbance *vs.* wavelength. The release of CLO from the wet-spun fibers was assessed in PBS after 1, 2, 4, 6 and 24 h. The selection of such medium was based on previous research studies from our team, in an attempt to approximate that of physiological-like media, also considering the desired future application of this system as a wound dressing.[7,10] Samples of CLO-containing fibers weighing 10 mg each were left in contact with 1 mL of PBS at 37 °C and 120 rpm, and aliquots of 150 μL were collected at each time point. Their absorbances were then measured in the range 200–900 nm. The release of CLO was determined by the differences in absorbance between the first moment of interaction (0 h) and the subsequent measuring periods, up to the 24 h mark.

2.4. AAPV-loaded fibers' inhibitory effect against HNE

AAPV-loaded and unloaded fibers were incubated in 1 mL of PBS, pH 7.4, at 37 °C and 120 rpm for 1, 2, 4, 6 and 24 h. After each incubation period, aliquots of 150 μL were collected; these represented the testing solutions. AAPV-unloaded fibers were also analyzed, in this way subtracting the polymers' influence from the results of AAPV-loaded fibers. HNE inhibition experiments were conducted as described in ref. 7. Briefly, a substrate solution (N-MeO-Suc-Ala-Ala-Pro-Val-*p*-NA) (125 μL) was mixed with 0.1 M Tris–HCl buffer (405 μL), along with the 150 μL aliquots of the testing solutions in PBS and 20 μL of HNE solution (45 mU). After 1 h of incubation at 37 °C, an inhibitor solution (500 μL) was added to stop the reaction and absorbances were read at 405 nm (EZ Read 2000 Microplate Reader, Biochrom, Cambridge, UK). Data were reported as maximum inhibitory concentration (IC_M). Experiments were conducted in triplicate, with three absorbance readings being done per replicate (mean averaging nine measurements).

2.5. Antioxidant activity

Free radical-scavenging activity was determined using the 1,1-diphenyl-2 picrylhydrazyl (DPPH) assay. Samples of 10 mg of each wet-spun fiber typology were immersed in 1 mL of absolute ethanol and incubated at 37 °C and 120 rpm for 1, 2, 4, 6 and 24 h. Ethanol was selected, not only because of the EO's high solubility, but also due to its common use in DPPH assays and the low water content, which could lead to interferences in the absorbance readings.[29–31] Aliquots of 10 μL were collected at each time period and mixed, in a 96-well plate, with 140 μL of a DPPH stock solution (400 μM in absolute ethanol). DMSO and Trolox were used as negative and positive controls, respectively. The absorbances were monitored every 5 min for 1 h and measured at 515 nm, using an EZ Read 2000 Microplate Reader (Biochrom, Cambridge, UK). Experiments were conducted in triplicate and data were reported in terms of the percentage of reduced DPPH at a steady state, which was calculated as follows (eqn (1)):

$$\mathrm{DPPH_r}\ (\%) = \frac{A_i - A_r}{A_i} \times 100, \quad (1)$$

in which A_r represents the absorbance registered at a steady state and A_i corresponds to the initial absorbance.

2.6. Bacteria inhibition: time-kill kinetics

Time-kill kinetics tests were conducted according to standard ASTM E2149-01, adapted as reported previously.[7,10] The antibacterial profile of the triaxial wet-spun fibers containing the AAPV peptide and the CLO was evaluated against 1×10^5 CFUs per mL suspensions of *S. aureus*, *S. epidermidis* and *E. coli* in TSB, and a suspension of *P. aeruginosa* prepared in NB. Samples of 10 mg were immersed in 1 mL of each bacterium suspension and incubated at 37 °C and 120 rpm for 1, 2, 4, 6 and 24 h. At each time point, bacterial suspensions were serially diluted in PBS (10^{-1} to 10^{-4}), plated in TSA and NA, and incubated at 37 °C for 24 h. Grown colonies were counted, and results were expressed in percentage (%) of bacteria inhibition. All measurements were performed in triplicate (three measurements were done per replicate, with data averaging nine values) and data were processed using the GraphPad Prism 8.0 software.

2.7. Biofilm formation

Bacteria inoculums of *S. aureus*, *S. epidermidis* and *E. coli* were prepared in TSB and of *P. aeruginosa* in NB and left overnight to grow at 37 °C and 120 rpm. Four replicates from each fiber typology (10 mg) were weighed into 48-well plates and covered with 5 μL of each inoculum mixed with 500 μL of MHB. Control wells containing the diluted inoculums but without samples were also considered for this assay. The plates were incubated for 48 h at 37 °C to allow biofilm formation. Afterwards, fibers were removed from each well and the plate was washed 3× with PBS to remove loosely bound biofilm cells. The plate was left at 37 °C for 20 min for fixating the biofilms. Then, a 0.1% w/v crystal violet (CV) aqueous solution was added to each well and the plate was left at RT for 15 min. This was followed by 3 washes with PBS to remove unbound CV. Finally, 500 μL of a 30% v/v acetic acid solution were added to each well for 15

min and aliquots were transferred to a 96 well-plate for absorbance readings at 595 nm.

2.8. Cytocompatibility testing

2.8.1. Cell culture conditions. The cytocompatibility and cell proliferation of all fiber typologies towards mouse embryonic fibroblast cell line (NIH 3T3) and human keratinocyte cell line (HaCaT) were evaluated using a direct contact assay. Cells were thawed and sub-cultured in DMEM supplemented with 10% v/v inactivated FBS (30 min, 56 °C) and 1% v/v penicillin–streptomycin, at 37 °C in a humidified atmosphere of 5% CO_2. Thereafter, cells were chemically detached from cell culture flasks using trypsin–EDTA solution. The number of cells was determined using a Malassez cell (Marienfeld, Germany), with cells being labelled with trypan blue (Sigma Aldrich, UK), to evaluate the proportion of dead cells, and counted using a Carl Zeiss Suzhou Co., Ltd (Suzhou, China) microscope. Cells were seeded in 96-well flat-bottom tissue plates (Greiner, Germany) and incubated for 24 h at 37 °C in a humidified atmosphere of 5% CO_2. HaCaT and NIH 3T3 were seeded at 15 000 and 20 000 cells per well, respectively (concentrations determined in a previous investigation; unpublished data). The experiments were performed using fibroblast cell line in passages 2 to 12 and keratinocyte cell line in passages 20 to 30. Fibrous samples of 2 mg were used for each test. Experiments were conducted in triplicate. Fibers were washed and disinfected 3× with deionized water (dH_2O) and 1× ethanol at 70% v/v, during 5 min each, prior to any testing.

2.8.2. Cell viability assessment. Prior to any fiber testing, the determination of the optimum cell number was carried out by seeding cells into 96-well flat black tissue plates at concentrations ranging from 5000 to 25 000 cells per well. Cells were incubated overnight at 37 °C and 5% CO_2 atmosphere. Afterwards, the medium was removed and 100 μL of a 10% v/v Alamar Blue™ (Invitrogen) were added to each well. Cells were again incubated for 1 h and the fluorescence was read (λ_{exc} = 560 and λ_{em} = 590 nm) using a Tecan fluorimeter (Tecan Spark, Lyon, France) with Tecan Spark Control 3.2 software. The metabolic activity for each cell concentration was calculated using eqn (2):

$$\text{Metabolic activity (\%)} = \frac{\text{Flu sample} - \text{Flu negative control}}{\text{Flu positive control} - \text{Flu negative control}} \times 100, \quad (2)$$

where the Flu sample corresponds to the fluorescence of each sample, Flu negative control corresponds to cells grown in 5% v/v DMSO solution, and Flu positive control represents a seeding of 50 000 cells per well, superior to the maximum tested density in the assay to assure that a very high growth of both cell lines was achieved.

After determining the optimum cell number for each cell line, cells were seeded and 6 h later fibers were added to the wells. After 24 and 48 h of incubation at 37 °C and 5% CO_2 atmosphere, the metabolic activity of the cells was evaluated using the Alamar Blue assay.

2.8.3. Cell lysis assessment. The cell lysis test was performed by following the instructions from LDH kit (Invitrogen). Firstly, the optimum cell number for performing the LDH assay was determined by seeding cells at concentrations from 0 to 10 000 cells per well in 96-well flat black tissue plates (6 replicates for each cell concentration). Cells were incubated overnight at 37 °C and 5% CO_2 atmosphere. Afterwards, 10 μL of sterile water were added to the first three replicates of each cell concentration (spontaneous LDH activity), whereas 10 μL of 2% v/v Triton solution in DPBS were added to the second set of replicates for each cell concentration (maximum LDH activity). Cells were again incubated for 45 min, protected from light, followed by the transfer of 50 μL of each supernatant to a new plate, to which 50 μL of a reaction mixture was added. Cells were once more incubated at room temperature (RT) during 10 min, protected from light. Then, 50 μL of a stop solution were added to all wells and the fluorescence was measured (λ_{exc} = 560 and λ_{em} = 590 nm) using Tecan fluorimeter. The maximum LDH release activity absorbances minus the spontaneous LDH release absorbances *versus* the tested cell numbers were plotted using the GraphPad Prism 8.0 software.

Cells were then seeded at the determined optimum cell number and, 6 h later, fibers were added. After 24 h of incubation, the cell lysis test was repeated. The percentages of cell lysis were then determined using the following eqn (3):

$$\text{Cell lysis (\%)} = \frac{\text{Fluo sample} - \text{Fluo spontaneous ctrl}}{\text{Fluo maximum ctrl} - \text{Fluo spontaneous ctrl}} \times 100, \quad (3)$$

where the Fluo sample corresponds to the fluorescence of cells treated with each fibrous sample, Fluo spontaneous ctrl represents the cells treated with sterile dH_2O (spontaneous LDH activity) and Fluo maximum ctrl corresponds to the cells treated with 2% v/v Triton (maximum LDH activity).

2.8.4. Cell morphology observations. Cells were visualized at brightfield using a light microscope (Carl Zeiss Suzhou Co., Ltd). Light microscope images were obtained at the beginning of the experiment (t = 0 h) and after 24 h of incubation in contact with the samples, to detect any possible changes in cell morphology. The images were acquired at a 10× magnification objective using an Axiocam 105 color camera (Zeiss, Switzerland), using a Zeiss ZEN 3.8 software.

2.9. Cell migration

2.9.1. Cell culture. Immortalized HaCaT were cultured in DMEM, supplemented with 10% v/v FBS and 1% v/v antibiotic–antimycotic solution. Cellular subcultures were performed when confluence reached values close to 80–90%. HaCaT cells were maintained in 25 cm^2 or 75 cm^2 tissue culture flasks in an incubator at 37 °C in a humidified atmosphere with 5% CO_2. The cell culture medium was renewed 2× per week. For subcultures and plating, the adherent cells were detached with trypsin solution 0.05% v/v, and fresh medium was added in order to neutralize the trypsin. The cell suspension was centrifuged 5 min at 160 g. The supernatant was discarded, and

fresh medium was added to obtain a new cell suspension. The cell suspension was injected in a Neubaeur chamber, and the cell concentration was determined.

2.9.2. Scratch assay. The effect of PCL/SA/CA, PCL/SA–AAPV/CA, PCL–CLO/SA/CA and PCL–CLO/SA–AAPV/CA samples on the migration profiles of HaCaT cells was evaluated by microscopic visualization after the scratch assay. Fibers were washed and disinfected 3× with dH_2O and 1× with ethanol at 70% v/v, during 5 min each, prior to the experiment.

Cells were seeded at a density of 5.0×10^4 cells per well, on a 24-well tissue culture plate (Trasadingen, Switzerland) the day before the experiments. After confirmation of cell confluency, a scratch on the cell monolayer was performed with the help of a disposable standard 200 μL pipette tip. The wells were washed with sterile PBS and fresh medium was added to the wells prior to the visualization and recording of the scratch in a Leica DMI 3000 B inverted fluorescence microscope (Heerbrugg, Switzerland) equipped with Leica DFC450 *C* camera (Heerbrugg, Switzerland). The cells were then exposed to the samples and were further incubated at 37 °C in a humidified atmosphere of 5% CO_2. Cells incubated only with fresh culture medium were used as control of cell migration. At the end of 24 and 48 h of contact, the cell migration was evaluated by microscopic visualization (phase contrast, 10× magnification) and determined using the ImageJ® software (version 1.53, National Institutes of Health, Bethesda, Maryland, USA), respectively. The percentages of wound area were determined at 24 h and 48 h, using the following eqn (4):[32]

$$\% \text{ wound area} = \frac{A(t)}{A_0} \times 100, \quad (4)$$

where $A(t)$ corresponds to the area of each sample determined at 24 h/48 h and A_0 corresponds to the area of each sample at t = 0 h.

2.10. Statistical analysis

All measurements were conducted in triplicate unless otherwise mentioned in the experimental sections. Numerical data were reported as mean ± standard deviation (SD). Data were treated using GraphPad Prism 8.0 Software (GraphPad Software Inc, USA). Normality analysis was performed, and results were analyzed using One-way ANOVA and Tukey tests. Statistically significant differences were considered at $p < 0.05$.

3. Results and discussion

The triaxial wet-spun fibers were produced *via* wet-spinning, as described in Section 2.2. The presence of three distinct layers on the fibers was confirmed *via* brightfield microscopy and scanning electron microscopy (SEM; Fig. 1). Through

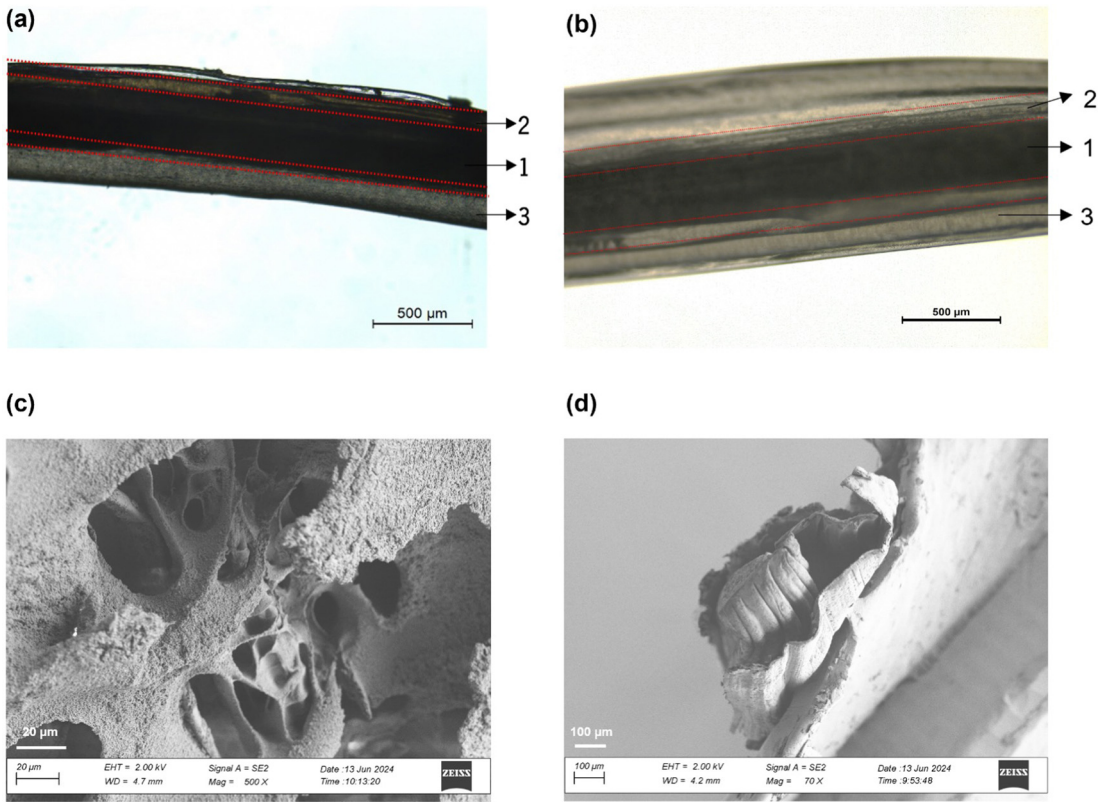

Fig. 1 Micrographs of triaxial wet-spun fiber morphology obtained *via* brightfield microscopy of (a) the complete system (1: core composed of PCL–CLO; 2: intermediate layer composed of SA–AAPV; 3: shell composed of CA); and (b) of the tri-axial fibers without additives (1: core composed of PCL; 2: intermediate layer composed of SA; 3: shell composed of CA). Visualization of the (c) surface morphology (magnification of 500×) and (d) cross-section (magnification of 70×) of the complete triaxial fibers obtained by SEM.

morphological, mechanical and thermal property analyses (data under peer revision), the flexibility and elasticity of the fibers was demonstrated, reaching values up to ≈300% of maximum elongation. Also, the engineered triaxial fibers were deemed highly stable when exposed to physiological-like media, during 28 days of incubation, losing only 23% in mass throughout that period. In the end, the triaxial wet-spun fibers were proven effective for knitting a wound dressing, in this way assuring the suitability of this system for wound healing applications.

The current work focused on the biological properties of the triaxial system, including antimicrobial and antioxidant activities, the release profiles of the active agents (AAPV and CLO), the regulation of the local enzymatic activity, and the cytocompatibility of each fiber typology (safety).

3.1. WAAPV release kinetics

In order to map AAPV release from peptide-loaded wet-spun fibers, a modified version of AAPV, in which a tryptophan was attached to the N-terminus, was used (WAAPV). Such modification was necessary due to an overlap of maximum absorbance bands from PCL, SA and CA polymers, centered at ≈200 nm, detected *via* UV-visible spectroscopy. As a result, WAAPV presented a maximum fluorescence peak at ≈275 nm, detected using fluorimetry, thus allowing for reliable detection of this compound without any interference from the remaining fiber compounds (confirmed by the analysis of the unloaded fibers).

Cumulative release profiles of WAAPV were determined by comparison with the calibration curve of the analyzed peptide (Fig. 2). SA–WAAPV monolayered fibers attained the highest release profiles, since no inner or outer layers were present to protect the payload, leading to a higher exposure of the peptide to the media. In its presence, the inner layer made of PCL or PCL–CLO conditioned the peptide release from both PCL/SA–WAAPV (difference of ≈3.25% compared to SA–AAPV) and PCL–CLO/SA–WAAPV coaxial fibers (difference of ≈7.04% compared to SA–AAPV). As observed in a previous research,[7] PCL tends to partially incorporate the SA or SA–WAAPV intermediate layers, interfering with the possible migration of the peptide towards the surrounding media. However, in this combination, the presence of visible folds and breakable sites along the SA–WAAPV shell (Fig. S1 in the ESI†) may have potentiated its degradation, accelerating peptide release. Moreover, the partial dissolution of SA while in contact with the physiological media in response to its highly hydrophilic nature and increased affinity towards water may also justify such outcome.[33,34]

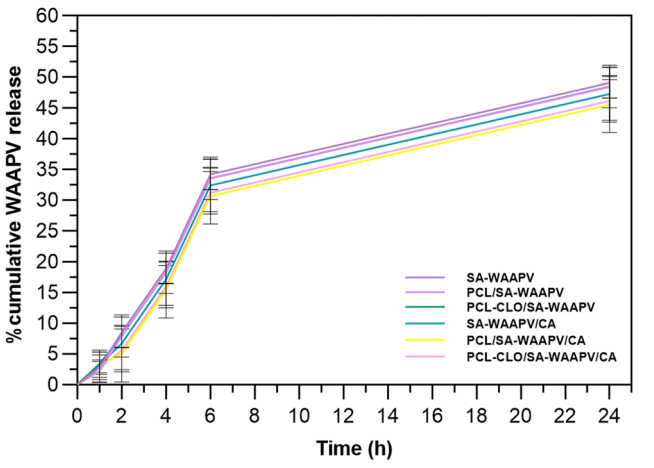

Fig. 2 Cumulative release kinetics of WAAPV-loaded wet-spun fibers. Data are reported as mean ± SD (n = 3). Statistical significance was determined *via* the Tukey test, applying multiple comparisons between the different fiber typologies (no statistical significances were detected).

PCL/SA–WAAPV/CA triaxial fibers reported the lowest WAAPV release profiles, since it was conditioned by both the innermost layer of PCL and an outermost layer made of CA, which was endowed with high mechanical resistance and hydrophobic behavior, limiting the interactions of WAAPV with water molecules from PBS.[35–37] That same conclusion could be retained to explain the low release profiles registered for SA–WAAPV/CA coaxial fibers. On the other hand, PCL–CLO/SA–WAAPV/CA triaxial fibers showed a slightly superior release rate compared to PCL/SA–AAPV/CA triaxial fibers (≈7.70% of increment). The presence of CLO, a compound with high affinity towards PCL, is expected to have altered the conformation of PCL polymeric chains, leading to a lower partial incorporation of the SA–WAAPV intermediate layer, therefore facilitating access to the peptide from the physiological media.[13] Overall, all WAAPV-loaded fibers displayed a prolonged and sustained release of the peptide, assuring their suitability as effective drug delivery platforms. Even though the mechanism of action of WAAPV is not yet fully understood, it is plausible to assume a similarity with AAPV, since both peptides share equal amino acids, apart from tryptophan.

3.2. CLO release profile

CLO's release kinetics was assessed after fiber contact with PBS up to 24 h of incubation (Fig. 3). Data from unloaded fibers were also collected to eliminate interference of polymers from the CLO-loaded fiber results. As expected, the PCL–CLO monolayered fibers release the most CLO in the shortest period of time, because of the easier access to the oil by the surrounding media.[22,38] Interestingly, both PCL–CLO/SA and PCL–CLO/SA–AAPV coaxial fibers also reached similar outcomes. One plausible explanation for this occurrence may rely on the feeble mechanical properties and media instability of the SA and SA–AAPV outer layers.[39] It is likely that the reduced structural integrities along with the hydrophilic character of the outer layers in both PCL–CLO/SA and PCL–CLO/SA–AAPV coaxial fibers caused the partial dissolution of SA and SA–AAPV onto the physiological media and, thus, prompted the release of CLO.[33,34] As CA displays high rigidity and structural integrity, conferring a barrier effect on the wet-spun fibers, PCL–CLO/CA and the triaxial fibers reported a slower release kinetics for CLO.[22,38,40] Generally, all fiber typologies experienced a burst release after 1 h of incubation, continuously increasing the CLO liberation from that point and until the 6 h mark. After that period oil release became more sustained, most likely because

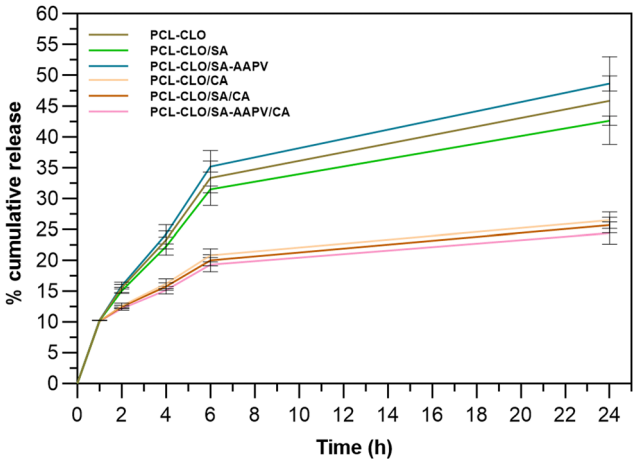

Fig. 3 Cumulative release kinetics of CLO-loaded wet-spun fibers. Data are reported as mean ± SD (n = 3). Statistical significance was determined *via* the Tukey test, applying multiple comparisons between the different fiber typologies (no statistical significances were found).

access to the remaining molecules was more challenging (stronger interactions with the polymers).

3.3. HNE inhibition

The inhibition of the HNE activity by AAPV-loaded wet-spun fibers was assessed by their incubation in PBS at 37 °C for a period of 24 h, simultaneously confirming the successful incorporation of the peptide (Fig. 4). Data from unloaded fibers was also collected and subtracted from the results from AAPV-loaded fibers, thus removing the polymer interference. All fibers presented HNE inhibitions superior to 15% in their first hour of incubation, which was associated with an initial burst release of the peptide (Fig. 2). However, after 6 h and until the 24 h mark, all samples reported a smaller inhibitory profile, since the peptide was released at a slower pace (Fig. 3).

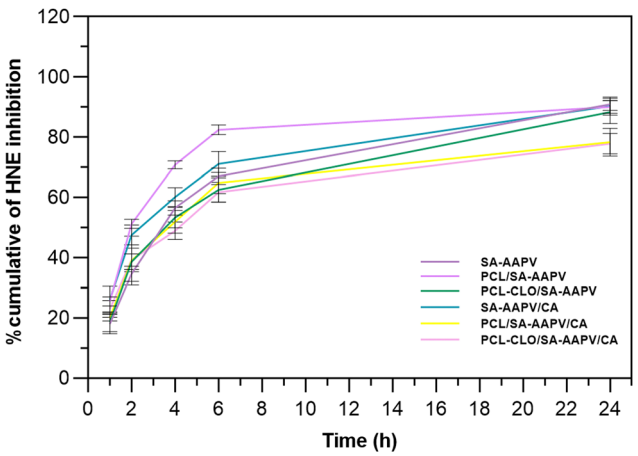

Fig. 4 HNE inhibition profile from AAPV-loaded wet-spun fibers. Data are reported as mean ± SD (n = 3). Statistical significance was determined *via* the Tukey test, applying multiple comparisons between the different fiber typologies (no statistical significances were found).

As expected, triaxial fibers reported lower HNE inhibitory capacities in comparison with coaxial and monolayered fibers, due to the presence of the CA protective layer, which limited the access to AAPV.[22,38,40] Additionally, in the presence of PCL, SA is partially lost, becoming entrapped in the PCL polymer chains, therefore interfering with the availability of AAPV and its release to the media.[7] That same theory explains not only the superior HNE inhibition from SA–AAPV/CA coaxial fibers, but also the lower HNE inhibitory profiles observed for PCL–CLO/SA–AAPV coaxial fibers. Since the affinity between CLO and PCL is greatly promoted by the interaction between the hydroxyl groups of eugenol (one of the main elements of CLO) and the carbonyl groups of PCL, leading to the molecular dispersion of CLO throughout the PCL polymeric matrix, the incorporation of the SA–AAPV intermediate layer was exacerbated.[13,41] However, after 6 h, such differences were less pronounced, most likely due to the characteristic high volatility of the EOs.[9,13] Despite inducing a smaller HNE inhibitory profile (in average), the triaxial fibers did not report significant differences compared to the other samples, being still classified as efficient in regulating HNE activity, with inhibitory capacities up to ≈65%, and thus capable of contributing to the healing process.[6]

3.4. Antioxidant activity

The antioxidant activities of CLO-loaded fibers were evaluated by incubating the samples for 24 h in absolute ethanol, prior to conducting the DPPH radical scavenging assay (Fig. 5 and Fig. S2 in the ESI†). Again, data from unloaded fibers were collected to remove the polymer interference in the results.

CLO's strong antioxidant properties originate in eugenol, one of its main components.[31] Brand-Williams *et al.* showed that the scavenging activity of eugenol is achieved by the initial formation of an antioxidant radical, followed by three types of reaction pathways, including the donation of a second hydrogen atom to the DPPH radical, the formation of a complex between one DPPH radical and one aryl radical, and the dimerization between two phenoxyl radicals that regenerate two hydroxyl groups capable of interacting with DPPH.[42] Eugenol's ability to interfere with free radicals from hydrogen peroxide offers cell protection against oxidative stress, which, consequently, accelerates wound healing.[43]

PCL–CLO monolayered fibers reached one of the highest DPPH reduction rates (varying between ≈57.87% at 2 h, the maximum, and ≈36.34% at 4 h, the minimum activity). This occurred because of the absence of an outer, protective barrier, therefore increasing the availability and exposure of CLO to the media.[22,38] PCL–CLO/SA and PCL–CLO/SA–AAPV coaxial fibers also reported high antioxidant activities, because of the SA and SA–AAPV outer layers mechanical limitations, along with their partial incorporation by PCL, which facilitated access to the oil and resulted in higher releases in comparison with CA-containing fibers (Fig. 3).[7] As expected, PCL–CLO/CA and the triaxial fibers reported the lowest antioxidant profiles confirming the protective functions of the CA shell.[22,38,40] Both the triaxial constructs and the PCL–CLO/CA coaxial fibers

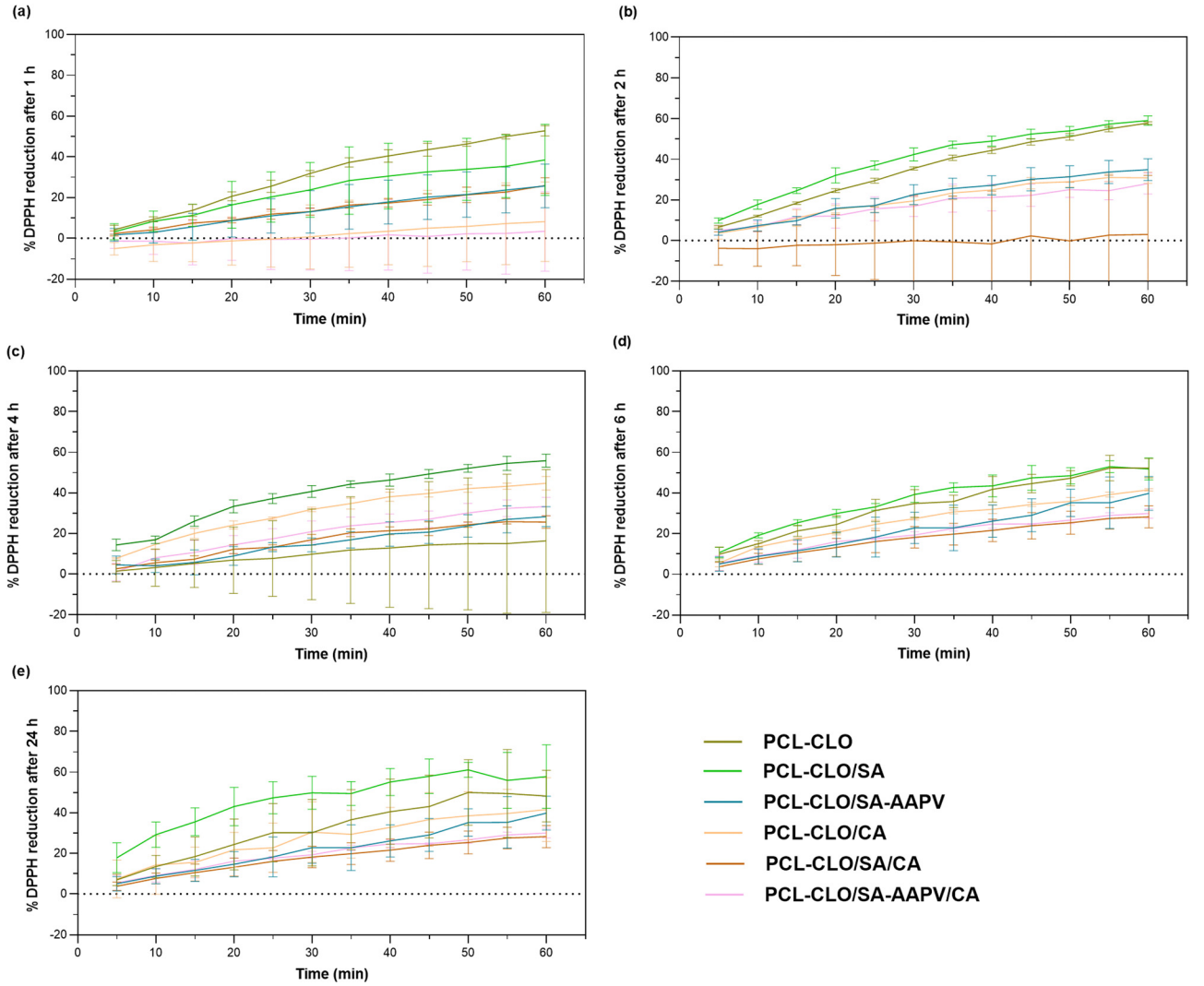

Fig. 5 DPPH reduction induced by CLO-loaded wet-spun fibers after (a) 1, (b) 2, (c) 4, (d) 6 and (e) 24 h of incubation. Data are reported as mean ± SD (n = 3). Statistical significance was determined *via* the Tukey test, applying multiple comparisons between the different fiber typologies (1 h: $p < 0.030$ significance between PCL and PCL–CLO/SA–AAPV/CA; 2 h: no statistical significances detected; 4 h: $p < 0.030$ significance between PCL–CLO/SA, PCL–CLO/SA–AAPV and PCL/SA/CA, PCL–CLO/SA/CA, PCL/SA–AAPV/CA, PCL–CLO/SA–AAPV/CA; 6 h: $p < 0.030$ significance between PCL–CLO and PCL–CLO/SA–AAPV, PCL–CLO/CA and PCL–CLO/SA/CA; 24 h: $p < 0.002$ significance between PCL–CLO, PCL–CLO/SA, PCL–CLO/SA–AAPV and PCL/SA/CA, PCL–CLO/SA/CA, PCL/SA–AAPV/CA, PCL–CLO/SA–AAPV/CA).

demonstrated antioxidant abilities overtime (in average 6.89–56.67%, 1.51–34.30% and 1.87–32.49% for PCL–CLO/CA, PCL–CLO/SA/CA and PCL–CLO/SA–AAPV/CA fibers, respectively), making them suitable for their intended application.

3.5. Antibacterial testing

S. aureus, *S. epidermidis*, *E. coli* and *P. aeruginosa* growth inhibition was evaluated after 24 h of exposure to the fibers at 37 °C (Fig. 6). Results showed that the antibacterial activity increased after the first hour of incubation, a clear effect of the CLO initial burst release (Fig. 2). CLO-loaded fibers achieved higher antibacterial efficacy in comparison with unloaded fibers. Such an occurrence was predicted since many reports have addressed that CLO's strong antibacterial properties as a result of one of its main elements, eugenol.[43,44] In fact, according to the literature, the CLO mechanism of action is based on its accumulation at the bacteria cell surfaces, disrupting the cytoplasmic membrane function and integrity, consequently leading to the leakage of cell content and cell death.[9,11]

PCL–CLO monolayered fibers reported superior antibacterial activities due to the larger availability and exposure of CLO to the media as was also evidenced in the release kinetics and DPPH reduction profiles (Fig. 2 and 4). PCL–CLO/SA and PCL–CLO/SA–AAPV coaxial fibers promoted one of the largest inhibitions of bacteria activity, once more due to the feeble structural integrity of the SA layer, in which polymer fragments could have been released and partially dissolved in the media. This way, the fibers' outer layer no longer restricted the access to the EO loaded into the fibers, explaining their antibacterial activity.[45] In contrast, the antibacterial effectiveness of PCL–CLO/CA

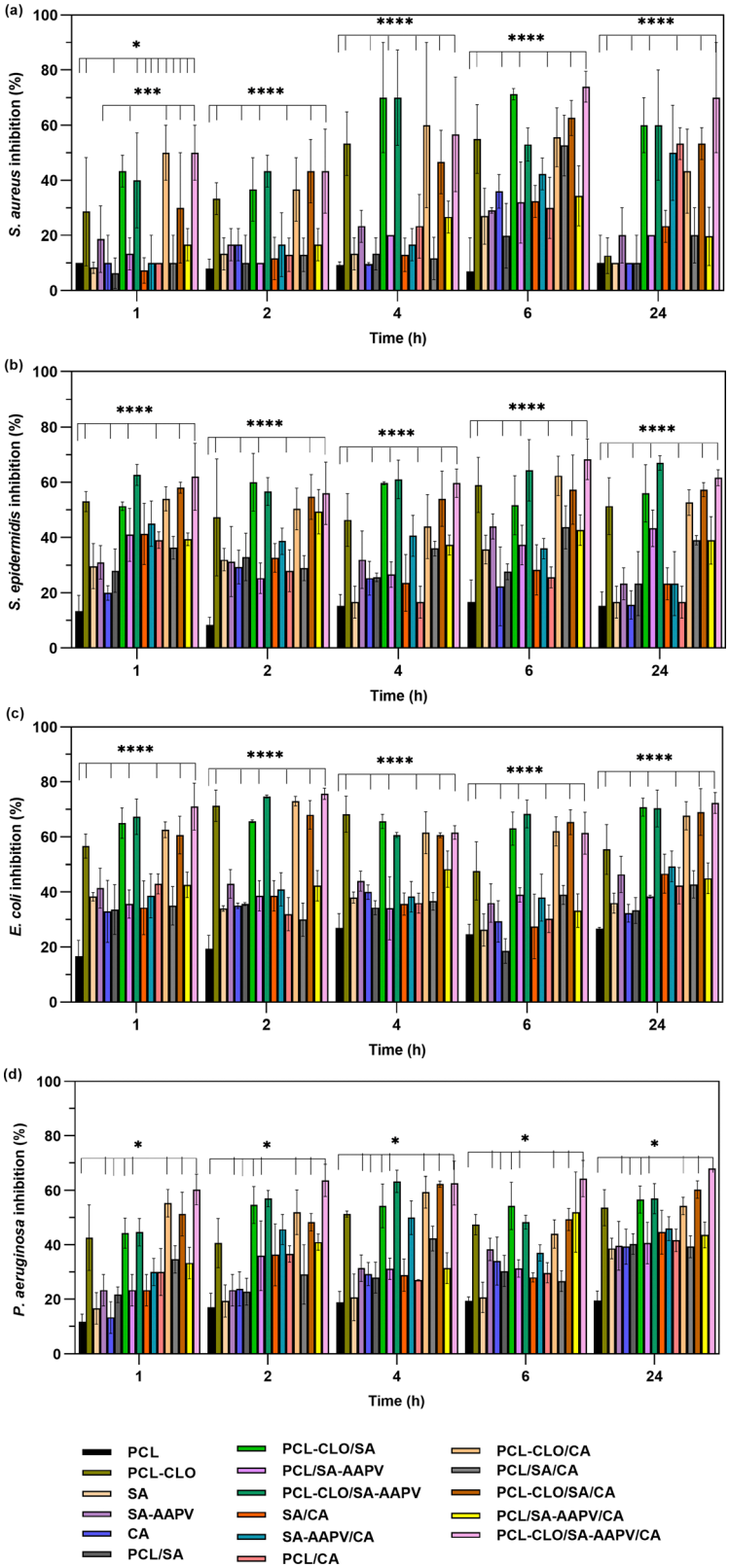

Fig. 6 Inhibition of (a) *S. aureus*, (*b*) *S. epidermidis*, (c) *E. coli* and (*d*) *P. aeruginosa* bacteria activities in contact with the engineered wet-spun fibers for a period of 24 h. Data are reported as mean ± S.D. (n = 3). Statistical significance was determined *via* Tukey tests applying multiple comparisons between each fiber typologies (*$p < 0.030$; **$p < 0.010$; ***$p < 0.001$; ****$p < 0.0001$).

coaxial fibers was reduced, since the CA outermost layer limited the release and interaction of CLO with the bacteria, as observed in the DPPH scavenging assay (Fig. 4).[22,38] Remarkably, AAPV-loaded fibers showed antibacterial activities above the samples without the peptide. Similar observations were made in a previous work conducted by our team, which reported AAPV ability to inhibit *S. aureus*; however, to date the mechanism of action is still undisclosed.[7] It is postulated that the peptide's antibacterial efficiency results from the presence of alanine (the precursor involved in its microbial synthesis is pyruvate) and proline (synthesized by α-ketoglutarate), both hydrophobic amino acids, frequently combined with antibiotics, and which antibacterial properties have already been discussed.[46,47] According to Xu *et al.* and De Jonge *et al.*, the mechanisms of action of peptides containing these amino acids in their structure, when combined with other active agents (*i.e.*, antibiotics), is associated with their infiltration through the microbial peptidoglycan layer, increasing its sensitivity.[47,48] In addition, peptides bearing proline have also shown inhibitory abilities against *P. aeruginosa* and *S. saprophyticus* strains activities,[49,50] causing membrane disintegration, more specifically, inhibiting the 70 kDa bacteria heat shock protein named DnaK present in such bacteria.[51] This premise may support the observed antibacterial activity promoted by PCL–CLO/SA–AAPV/CA triaxial fibers in comparison with PCL–CLO/SA/CA. Although synergistic effects arising from the conjugation of peptides and EOs are not yet well understood, several research studies have addressed the potential of such combinations as an alternative to antibiotics for fighting bacterial infections.[52,53]

The antibacterial activities observed for both CLO- and AAPV-unloaded fibers may be a result of the presence of residual Ca^{2+} salts from the coagulation bath.[54] Overall, the antibacterial abilities of CLO-loaded fibers were verified against the four tested bacteria, confirming the efficacy of the engineered system for addressing bacterial infections.

3.6. Biofilm formation

A qualitative biofilm formation assay was conducted to complement the evaluation of the fibers' antibacterial properties (Fig. 7 and Fig. S3 in the ESI†). Biofilms consist of a group of microorganisms condensed within a matrix, adhered to a living surface, and presenting different growth rates.[55] The formation of biofilms contributes to an increase in bacterial infection prevalence, more challenging to treat, which is frequently associated with CW escalation. Consequently, developing polymeric structures with antibiofilm formation properties is of utmost importance.[56]

AAPV and CLO-unloaded fibers reached elevated microbial counts (optical densities superior to 1.0). Several reports addressed high formation of biofilms in PCL structures produced using spinning techniques. According to Ruckh *et al.*, PCL electrospun scaffolds are usually ineffective towards inhibiting the growth of bacteria biofilms of both *P. aeruginosa* and *S. epidermidis*.[57,58] Similarly, Pompa-Monroy *et al.* observed dense *S. aureus* biofilms on PCL and curcumin electrospun fibers.[55] For this same reason, PCL has been recently addressed as a promising material for microbial biomass production.[59] Alginate has also been reported in several studies as a polysaccharide that promotes biofilm formation, acting as a molecular glue that enhances bacterial adhesion to the surfaces, maintaining the structures of the biofilms; hence, justifying the optical densities superior to 1.5 registered for SA and SA–AAPV hollow fibers.[60] CA is also not capable of hindering formation of bacteria biofilms.[61]

The presence of AAPV did not influence the results (*e.g.*, average optical density of PCL/SA–AAPV fibers was not significantly different from average optical density of PCL fibers), since the compound was loaded at low concentrations. However, CLO-loaded fibers attained reductions in optical density, thus showing inhibitory capacities towards the formation of biofilms. Several reports have disclosed the use of plant extracts for inhibiting biofilm formation.[55,62] Although its mechanism of action is not yet fully understood, cinnamaldehyde, one of the main components of CLO, has been classified as a quorum-sensing (QS) inhibitor, meaning that it is responsible for regulating the expression of genes essential for the formation of biofilms. The presence of EOs disrupts QS molecules, consequently reducing pathogenesis and biofilm formation.[55] Such an antibiofilm effect was highly pronounced in PCL–CLO monolayered fibers due to the highest exposure of the EO to the surrounding media (Fig. 3). Although in triaxial fibers the optical densities were higher in comparison with monolayered fibers, caused by the influence of the three tested polymers PCL, SA and CA (not capable of effective biofilm inhibitory properties), such samples still attained reductions in optical density of $\approx$73% in relation to pristine SA and CA fibers, showing a potential of the final engineered triaxial system for antibiofilm formation activities.

3.7. Cytocompatibility testing

The cytocompatibility and cell lysis induced by the engineered wet-spun fibers were evaluated after 24 h and 48 h of contact with HaCaT cells, seeded at 15 000 cells per well and 8000 cells per well, and with NIH 3T3 cells, seeded at 20 000 cells per well and 8000 cells per well, respectively for Alamar Blue and LDH tests (Fig. 8 and Fig. S4 in the ESI†).[63] The ISO standard 10.993-5:2009 regulation states that a cytotoxic effect is defined when the metabolic activity of cells decreases at least 30%.[64] Although results showed that SA and SA–AAPV hollow fibers reduced the metabolic activity of both cell lines by more than 30% (Fig. 6a–d), it is likely the SA polymer chains interfered with several pathways related to the metabolic activities of the cells, but not necessarily causing cell lysis. This conclusion can be supported by the small cell lysis observed for SA and SA–AAPV hollow fibers in both cell lines (cell lysis $<$23%; Fig. 8e and f). Such an occurrence was already predicted considering the low mechanical properties and water-affinity behaviors of SA and SA–AAPV layers, which underwent a partial dissolution in contact with the media, and, through that, interfered with essential nutrient exchanges for the survival of the cells.[65] In fact, as both SA and AAPV compounds present affinity towards

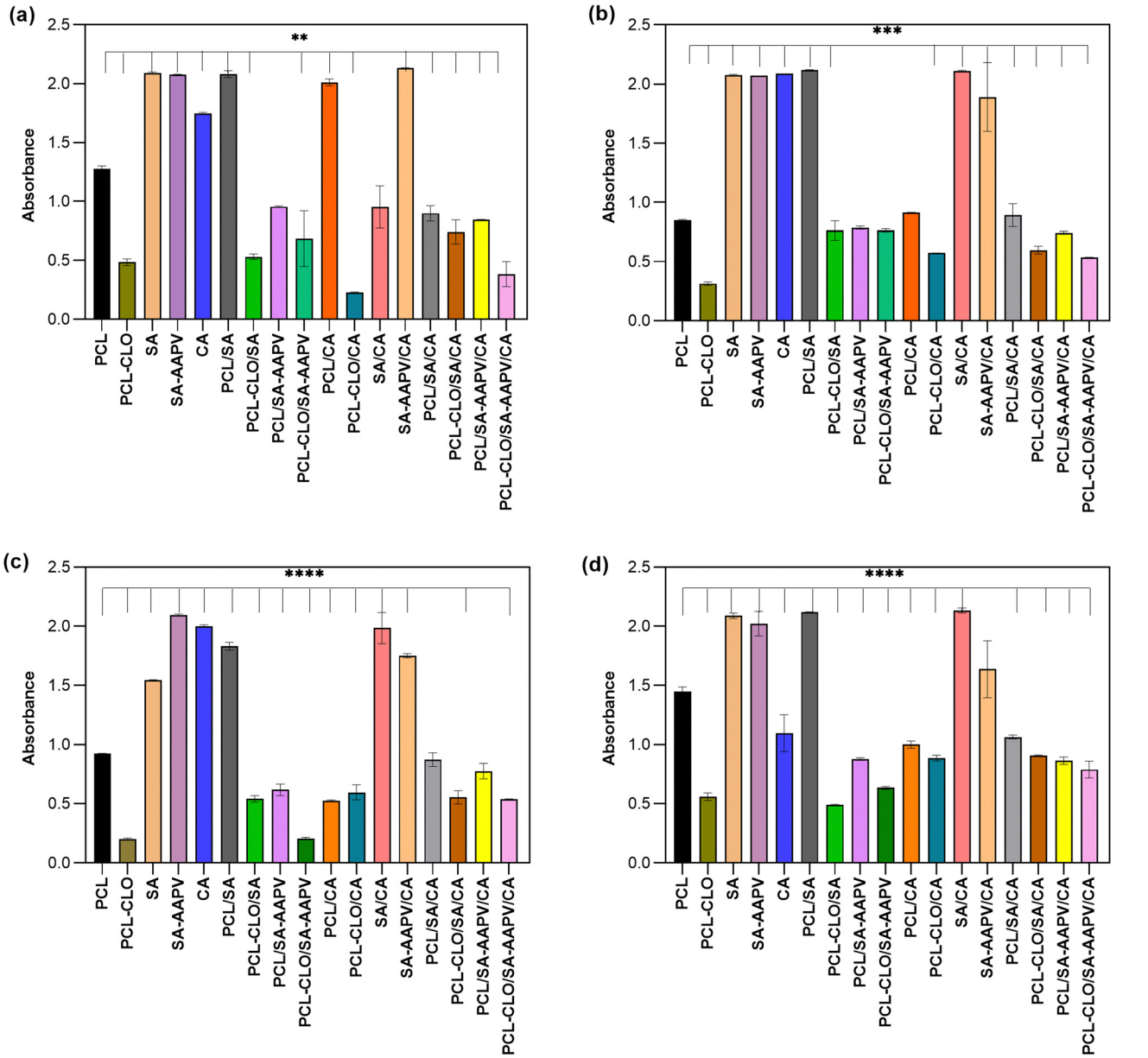

Fig. 7 Inhibition of (a) *S. aureus*, (b) *S. epidermidis*, (c) *E. coli* and (d) *P. aeruginosa* bacteria biofilms in contact with the engineered wet-spun fibers for a period of 48 h. Data are reported as mean ± S.D. (n = 3). Statistical significance was determined *via* Tukey tests applying multiple comparisons between PCL and the remainder fiber typologies (statistical significances were found between PCL and (a) PCL–CLO, SA, SA–AAPV, CA, PCL/SA, PCL–CLO/SA, PCL–CLO/SA–AAPV, PCL/CA, PCL–CLO/CA, SA–AAPV/CA and the triaxial fibers: **$p < 0.0053$; (b) PCL–CLO, SA, SA–AAPV, CA, PCL/SA, PCL–CLO/CA, SA/CA, SA–AAPV/CA and the triaxial fibers: ***$p < 0.0003$; (c) PCL–CLO, SA, SA–AAPV, CA, PCL/SA, PCL–CLO/SA, PCL/SA–AAPV, PCL–CLO/SA–AAPV, PCL/CA, PCL–CLO/CA, SA/CA, SA–AAPV/CA, PCL–CLO/SA/CA and PCL–CLO/SA–AAPV/CA: ****$p < 0.0001$; (d) PCL–CLO, SA, SA–AAPV, CA, PCL/SA, PCL–CLO/SA, PCL/SA–AAPV, PCL–CLO/SA–AAPV, PCL/CA, PCL–CLO/CA, SA/CA and the triaxial fibers: ****$p < 0.0001$).

PBS water molecules, protein adsorption was also likely hindered by this strong pre-existing interaction.[65,66] AAPV did not significantly influence the results, since its incorporation onto the fibers was done at a low concentration (50 μg mL^{-1}). Likewise, reports have shown that low molecular weight peptides loaded at small concentrations (<2048 mg mL^{-1}) into polymeric structures do not tend to show any toxic effects in mammalian cells.[67]

In turn, PCL was found to promote cell viability. As PCL is endowed with an hydrophobic character and reduced water affinity, the polymer did not limit any nutrient exchange, leading to high metabolic activity of both cell lines.[7,63,64] Additionally, as PCL is recognized by its excellent mechanical and elastic properties, there were no polymer fragments released onto the media that could have blocked essential pathways for cell survival.[65,66] Nevertheless, PCL's induced cytocompatibility was not sufficient to overcome the toxicity inherent to the SA and SA–AAPV shells, thus identifying PCL/SA, PCL–CLO/SA and PCL/SA–AAPV coaxial fibers with slightly toxic profiles.[66] Although the toxic effects of CLO towards

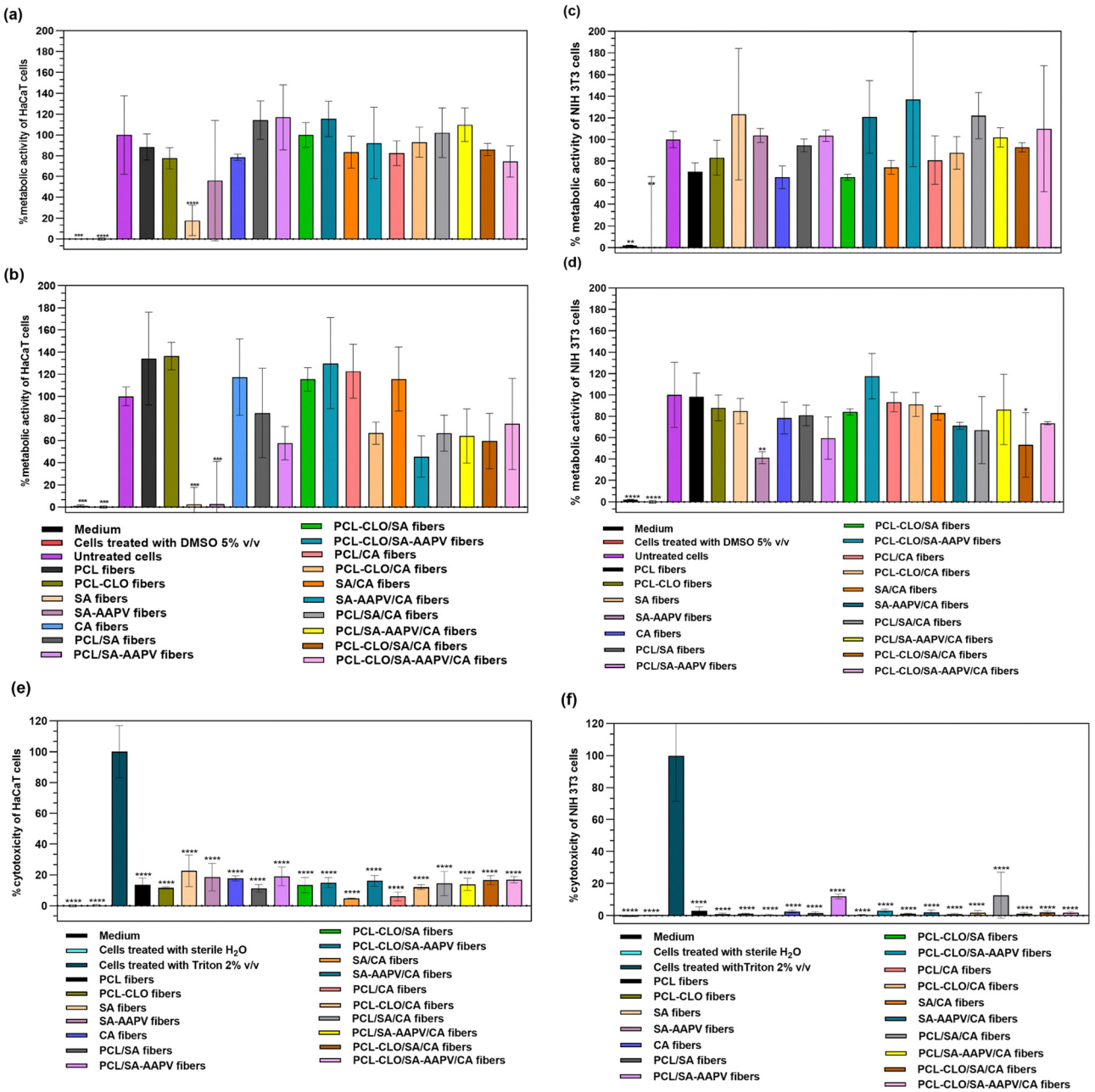

Fig. 8 Cytocompatibility evaluation of HaCaT and NIH 3T3 cells after (a), (c) 24 h and (b), (d) 48 h of contact with fibers, respectively; cell lysis evaluation of (e) HaCaT and (f) NIH 3T3 cells. Data are reported as mean ± S.D. (n = 3). Statistical significance was determined *via* the Dunnett test applying multiple comparisons between the different fiber typologies and each respective positive control (***$p < 0.0007$; ****$p < 0.0001$).

several cell lines have been extensively addressed in the literature,[68–70] here, CLO-loaded fibers achieved high metabolic activities (>92.18%). The structural integrity of the fibers, promoted by the oil affinity towards PCL, allowed for a sustained and prolonged release of the EO and potential polymeric fragments (Fig. 2); therefore, preventing any severe toxicological effect against the tested cell lines.[7,22] Additionally, the presence of CA also enhanced cells metabolic activities (Fig. 8a–d), corroborating the observations of previous studies.[71,72] The positive effects of both PCL and CA polymers were proven by the metabolic activities reported by the PCL/CA coaxial fibers in the range of 73.99 to 118.16%. Moreover, low cell lysis was registered, especially regarding the NIH 3T3 cell line (0.47–13.76%) (Fig. 8f). According to Hoh *et al.*, keratinocyte cell lines are more susceptible to cell lysis when exposed to toxic substances.[64] Fibers did not alter the characteristic morphology of the cells (Fig. S5 and S6 in the ESI†). Unlike the common shape of fibroblasts (flat and branch-shaped), NIH 3T3 cells showed a rounded shape, often an indication of an increased cells confluence (dependent on seeding).[73,74] All in all, apart from both SA and SA–AAPV hollow fibers, which function as control groups, the safety and suitability of each

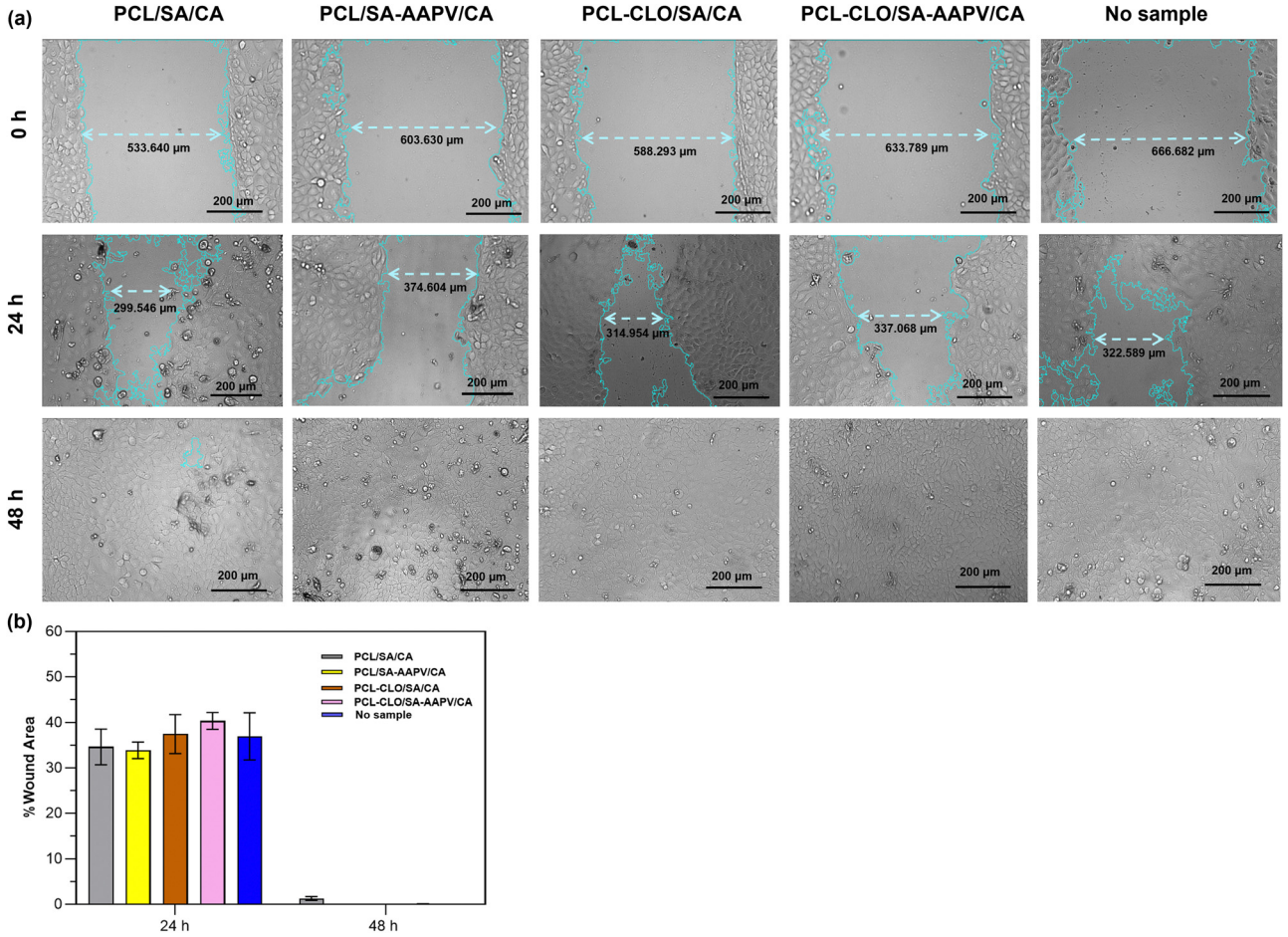

Fig. 9 Cellular migration evaluation *via* the scratch test: (a) time-lapse images of PCL/SA/CA, PCL/SA–AAPV/CA, PCL–CLO/SA/CA and PCL–CLO/SA–AAPV/CA samples collected after 0, 24 and 48 h of contact with HaCaT; (b) evolution of % wound area at 24 and 48 h. Data are reported as mean ± SD (n = 4). Statistical significance was determined *via* Tukey tests, applying multiple comparisons between the different fiber typologies (no statistical significances were found).

fiber typology was confirmed, including the final triaxial construct.

3.8. Cell migration

One of the key mechanisms of wound healing is the migration of epithelial cells from the extremities of a wound to its center, forming a new skin layer and sealing the wound.[75] Therefore, it is essential that cellular migration occurs in a timely manner, allowing for tissue remodeling and the wound progression throughout the following steps of healing.[76]

A scratch test involving the contact of HaCaT cells with each triaxial fibrous system for 48 h (Fig. 9) was conducted, to evaluate the fibers' potential for promoting cell migration. It was evident that a reduction of the wound areas was achieved by cell migration after the initial 24 h of contact in all tested samples, varying between 33.85 ± 1.81% and 40.33 ± 1.87% (absence of statistically significant differences).

PCL (one of the main fibers' components) has been frequently used for wound healing and tissue engineering applications due to its high biocompatibility, cytocompatibility, along with its capacity to enhance cellular proliferation and migration.[77] Additionally, according to research conducted by Yu *et al.* and Yilgor *et al.*, PCL-composite constructs have led to high migration of epithelial cells.[78,79] Similar outcomes have been attained for CA-containing nanofibers used in diabetic wound care.[80,81] Despite SA's high hydrophilicity interference with cell nutrient exchanges, decreasing the metabolic activity of keratinocytes (Fig. 8a), the presence of both PCL inner and CA outer layers prevented such outcomes from hindering HaCaT migration capacities. This is in accordance with previous works that showed the ability of SA blended with other polymers, such as polyacrylamide and polyvinyl alcohol, to increase the percentage of wound closure, enhancing the migration of fibroblasts.[82,83]

Even though AMPs present the potential to accelerate epithelial cell migration (*i.e.*, A-hBD-2; cathelicidin-DM), the presence of AAPV did not significantly influence the results. Once again, its small loading concentration (50 µg mL^{-1}) can explain the observations.[84,85] According to Daemi *et al.*, the presence of cinnamon extracts leads to an increase of the cyclin D1 (protein-coding gene) expression which, consequently, accelerates cell migration in wound sites.[86] However, as CLO

was loaded at a small amount and at the fiber core, showing a paced release profile through the fiber layers (Fig. 3), the CLO-loaded fibers attained similar wound area percentages at 24 h, compared to CLO-unloaded samples.

Apart from PCL/SA/CA samples, which still displayed a wound area percentage of ≈1.50% at the 48 h mark, all triaxial fibers reached a full wound closure during that time without inducing any HaCaT morphological changes, proving their capacities to enable cell migration in an appropriate period of time. Although the evolution of wound closure throughout the incubation time was similar to the control sample (without fiber addition), it is relevant to mention that the present triaxial fibers led to an improvement of HaCaT metabolic activity (Fig. 8a–d). The present outcomes not only prove the safety of the fibers, but also their potential to allow a successful healing process and increase the metabolic activities of epithelial cells, which are fundamental properties for future applications as wound dressings.

4. Conclusions

A triaxial wet-spun fibrous system loaded with AAPV and CLO was proposed in this research. The selected polymers, PCL, SA and CA, were deemed capable of loading the agents and sustaining their release *via* the porous structure at the fiber shell. The engineered fibers attained high HNE inhibitory capacities, good antioxidant activities, and inhibited the growth and biofilm formation of *S. aureus*, *S. epidermidis*, *E. coli* and *P. aeruginosa* bacteria, the four most prevalent in CW scenarios. Data from cytocompatibility analysis confirmed the safety of the triaxial fibers for potential human uses. Moreover, they allowed for an efficient cellular migration, which is essential for a successful healing process. In the end, an innovative drug delivery platform of three layers that combined simultaneously a peptide and an EO was attained, characterized by important antioxidant, antibacterial and enzymatic regulation activities, giving rise to an innovative solution for treating CWs. Further improvements in the mechanical properties of the triaxial wet-spun fibers will be required, as well as an evaluation of the synergistic mechanisms between the two active agents.

Data availability

The data supporting this article have been included as part of the ESI.†

Conflicts of interest

The authors declare no conflict of interest.

Acknowledgements

This work was funded by the European Regional Development Fund through the Operational Competitiveness Program and the National Foundation for Science and Technology of Portugal (FCT) under the projects UID/CTM/00264/2020 of the Centre for Textile Science and Technology (2C2T) on its components base (**https://doi.org/10.54499/UIDB/00264/2020**) and programmatic (**https://doi.org/10.54499/UIDP/00264/2020**), the project UID/QUI/00686/2020 of the Centre of Chemistry, on its base (**https://doi.org/10.54499/UIDB/00686/2020**) and programmatic (**https://doi.org/10.54499/UIDP/00686/2020**) components, and by the strategic programs UIDB/04469/2020 and LABBELS – Associate Laboratory in Biotechnology, Bioengineering and Microelectromechanical Systems, LA/P/0029/2020. C. S. M. and A. F. G. S. acknowledge FCT for PhD funding *via* scholarship 2020.08547.BD and 2022.11171.BD respectively, along with extra funding for conducting an international internship in Lyon. A. R. and H. P. F. also acknowledge FCT for auxiliary researcher contracts, respectively 2021.02803.CEECIND (DOI **https://doi.org/10.54499/2021.02803.CEECIND/CP1664/CT0018**) and 2021.02720.CEEIND.

References

1 H. P. Felgueiras and M. T. P. Amorim, Functionalization of electrospun polymeric wound dressings with antimicrobial peptides, *Colloids Surf., B*, 2017, **156**, 133–148, DOI: **10.1016/j.colsurfb.2017.05.001**.

2 K. Järbrink, G. Ni, H. Sönnergren, A. Schmidtchen, C. Pang, R. Bajpai and J. Car, Prevalence and incidence of chronic wounds and related complications: a protocol for a systematic review, *Syst. Rev.*, 2016, **5**, 1–6, DOI: **10.1186/s13643-016-0329-y**.

3 R. G. Frykberg and J. Banks, Challenges in the Treatment of Chronic Wounds, *Adv. Wound Care*, 2015, **4**, 560–582, DOI: **10.1089/wound.2015.0635**.

4 S. Phan, C. H. Feng, R. Huang, Z. X. Lee, Y. Moua, O. J. Phung and J. R. Lenhard, Relative Abundance and Detection of *Pseudomonas aeruginosa* from Chronic Wound Infections Globally, *Microorganisms*, 2023, **11**, 1210, DOI: **10.3390/microorganisms11051210**.

5 M. Plotczyk and C. A. Higgins, *Skin biology*, Elsevier Ltd, 2019, DOI: **10.1016/b978-0-08-102546-8.00001-7**.

6 F. C. Santos, A. M. S. Soares, M. S. T. Gonçalves and S. P. G. Costa, Phototriggered release of tetrapeptide AAPV from coumarinyl and pyrenyl cages, *Amino Acids*, 2017, **49**, 1077–1088, DOI: **10.1007/s00726-017-2405-6**.

7 C. S. Miranda, A. F. G. Silva, C. L. Seabra, S. Reis, M. M. P. Silva, S. M. M. A. Pereira-lima, S. P. G. Costa and H. P. Felgueiras, Sodium alginate/polycaprolactone *co*-axial wet-spun microfibers modified with *N*-carboxymethyl chitosan and the peptide AAPV for *Staphylococcus aureus* and human neutrophil elastase inhibition in potential chronic wound scenarios, *Biomater. Adv.*, 2023, **151**, 213488, DOI: **10.1016/j.bioadv.2023.213488**.

8 R. Alasbahi and M. Melzig, The in vitro inhibition of human neutrophil elastase activity by some yemeni medicinal plants, *Sci. Pharm.*, 2008, **76**, 471–484, DOI: **10.3797/scipharm.0804-25**.

9 J. C. Antunes, T. D. Tavares, M. A. Teixeira, M. O. Teixeira, N. C. Homem, M. T. P. Amorim and H. P. Felgueiras, Eugenol-containing essential oils loaded onto chitosan/polyvinyl alcohol blended films and their ability to eradicate *Staphylococcus aureus* or *Pseudomonas aeruginosa* from infected microenvironments, *Pharmaceutics*, 2021, **13**, 195, DOI: 10.3390/pharmaceutics13020195.

10 N. C. Homem, T. D. Tavares, C. S. Miranda, J. C. Antunes, M. P. Teresa and H. P. Felgueiras, Functionalization of crosslinked sodium alginate/gelatin wet-spun porous fibers with Nisin *Z* for the inhibition of *Staphylococcus aureus* – induced infections, *Int. J. Mol.*, 2021, **22**, 1930, DOI: 10.3390/ijms22041930.

11 C. S. Miranda, J. C. Antunes, N. C. Homem and H. P. Felgueiras, Controlled Release of Cinnamon Leaf Oil from Chitosan Microcapsules Embedded within a Sodium Alginate/Gelatin Hydrogel-Like Film for *Pseudomonas aeruginosa* Elimination, *Proceedings*, 2021, **69**, 39, DOI: 10.3390/cgpm2020-07181.

12 T. D. Tavares, J. C. Antunes, J. Padrão, A. I. Ribeiro, A. Zille, M. T. P. Amorim, F. Ferreira and H. P. Felgueiras, Activity of specialized biomolecules against Gram-positive and Gram-negative bacteria, *Antibiotics*, 2020, **9**, 1–16, DOI: 10.3390/antibiotics9060314.

13 H. P. Felgueiras, N. C. Homem, M. A. Teixeira, A. R. M. Ribeiro, J. C. Antunes and M. T. P. Amorim, Physical, thermal, and antibacterial effects of active essential oils with potential for biomedical applications loaded onto cellulose acetate/polycaprolactone wet-spun microfibers, *Biomolecules*, 2020, **10**, 1–20, DOI: 10.3390/biom10081129.

14 M. Chen, Y. Hu, J. Zhou, Y. Xie, H. Wu, T. Yuan and Z. Yang, Facile fabrication of tea tree oil-loaded antibacterial microcapsules by complex coacervation of sodium alginate/quaternary ammonium salt of chitosan, *RSC Adv.*, 2016, **6**, 13032–13039, DOI: 10.1039/c5ra26052c.

15 A. Marchese, R. Barbieri, E. Coppo, I. E. Orhan, S. F. Nabavi, M. Izadi, M. Abdollahi, M. Nabavi and M. Ajami, Critical Reviews in Microbiology Antimicrobial activity of eugenol and essential oils containing eugenol: a mechanistic viewpoint, *Crit. Rev. Microbiol.*, 2017, **43**, 668–689, DOI: 10.1080/1040841X.2017.1295225.

16 M. Bai, X. Jin, Z. Cen, K. Yu, H. Yu, R. Xiao, J. Deng, Z. Lai, H. Wu and Y. Li, GC–MS and FTIR spectroscopy for the identification and assessment of essential oil components of five cinnamon leaves, *Rev. Bras. Bot.*, 2021, **44**, 525–535, DOI: 10.1007/s40415-021-00751-7.

17 P. Knauth, Z. L. López, G. J. A. Hernández and M. T. E. Sevilla, Cinnamon essential oil: chemical composition and biological activities, *Biochemistry Research Trends*, 2018.

18 H. Leem, E. Kim, M. Seo and S. Choi, Antioxidant and Anti-Inflammatory Activities of Eugenol and Its Derivatives from Clove (*Eugenia caryophyllata* Thunb.), *J. Korean Soc. Food Sci. Nutr.*, 2011, **40**, 1361–1370, DOI: 10.3746/jkfn.2011.40.10.1361.

19 J. M. Domingues, M. O. Teixeira, M. A. Teixeira, D. Freitas, S. F. da Silva, S. D. Tohidi, R. D. V. Fernandes, J. Padrão, A. Zille, C. Silva, J. C. Antunes and H. P. Felgueiras, Inhibition of Escherichia Virus MS2, Surrogate of SARS-CoV-2, via Essential Oils-Loaded Electrospun Fibrous Mats: Increasing the Multifunctionality of Antivirus Protection Masks, *Pharmaceutics*, 2022, **14**, 303, DOI: 10.3390/pharmaceutics14020303.

20 C. S. Miranda, A. F. G. Silva, S. M. M. A. Pereira-Lima, S. P. G. Costa, N. C. Homem and H. P. Felgueiras, Tunable Spun Fiber Constructs in Biomedicine: Influence of Processing Parameters in the Fibers' Architecture, *Pharmaceutics*, 2022, **14**, 164, DOI: 10.3390/pharmaceutics14010164.

21 A. Mirabedini, J. Foroughi and G. G. Wallace, Developments in conducting polymer fibres: from established spinning methods toward advanced applications, *RSC Adv.*, 2016, **6**, 44687–44716, DOI: 10.1039/c6ra05626a.

22 A. Mirabedini, Developing novel spinning methods to fabricate continuous multifunctional fibres for bioapplications [Doctoral dissertation, University of Wollongong]. University of Wollongong Thesis Collections, 2017, https://ro.uow.edu.au/theses1.

23 Y. Jung, H. Yang, I.-Y. Lee, T.-S. Yong and S. Lee, Polymers Containing Cinnamon Oil: Their Antibacterial and Antifungal Properties and Acaricidal Effect against House Dust Mites, *Polymers*, 2020, **12**, 1–18, DOI: 10.3390/polym12010243.

24 U. G. P. P. Subasinghe and S. Wickramarachchi, Encapsulation of cinnamon leaf oil within chitosan: formulation and characterization, *Ceylon J. Sci.*, 2019, **48**, 279, DOI: 10.4038/cjs.v48i3.7652.

25 M. A. Teixeira, M. T. P. Amorim and H. P. Felgueiras, Cellulose Acetate in Wound Dressings Formulations: Potentialities and Electrospinning Capability, in: XV Mediterr. Conf. Med. Biol. Eng. Comput. – MEDICON 2019, Springer International Publishing, 2020, pp. 1515–1525, DOI: 10.1007/978-3-030-31635-8.

26 P. Boukamp, Normal Keratinization in a Spontaneously Immortalized, *J. Cell Biol.*, 1988, **106**, 761–771.

27 C. S. Miranda, E. Marinho, C. L. Seabra, C. Evenou, J. Lamartine, B. Fromy, S. P. G. Costa, N. C. Homem and H. P. Felgueiras, Antimicrobial, antioxidant and cytocompatible coaxial wet-spun fibers made of polycaprolactone and cellulose acetate loaded with essential oils for wound care, *Int. J. Biol. Macromol.*, 2024, **277**, 134565, DOI: 10.1016/j.ijbiomac.2024.134565.

28 C. S. Miranda, A. F. G. Silva, C. L. Seabra, S. Reis, M. M. P. Silva, S. M. M. A. Pereira-Lima, S. P. G. Costa, N. C. Homem and H. P. Felgueiras, Sodium alginate/polycaprolactone co-axial wet-spun microfibers modified with *N*-carboxymethyl chitosan and the peptide AAPV for *Staphylococcus aureus* and human neutrophil elastase inhibition in potential chronic wound scenarios, *Biomater. Adv.*, 2023, **151**, 213488, DOI: 10.1016/j.bioadv.2023.213488.

29 S. C. T. Nicklisch and J. H. Waite, Optimized DPPH assay in a detergent-based buffer system for measuring antioxidant activity of proteins, *MethodsX*, 2014, **1**, 233–238, DOI: 10.1016/j.mex.2014.10.004.

30 A. Sachett, M. Gallas-lopes, G. M. M. Conterato, A. P. Herrmann, A. Piato and A. Piato, Antioxidant activity by

DPPH assay: in vitro protocol, *Protocols*, 2021, 4–7, DOI: 10.17504/protocols.io.btbpnimn.

31 C. Sebaaly, A. Jraij, H. Fessi, C. Charcosset and H. Greige-Gerges, Preparation and characterization of clove essential oil-loaded liposomes, *Food Chem.*, 2015, **178**, 52–62, DOI: 10.1016/j.foodchem.2015.01.067.

32 E. Sarro, A. Victoria, P. Bobadilla, J. Are, H. M. Byrne, P. K. Maini, T. Carraro, S. Balocco and A. Meseguer, In vitro cell migration quantification method for scratch assays, *J. R. Soc., Interface*, 2019, 16–151, DOI: 10.1098/rsif.2018.0709.

33 M. Umar, A. Ullah, H. Nawaz, T. Areeb, M. Hashmi, D. Kharaghani, K. O. Kim and I. S. Kim, Wet-spun bi-component alginate based hydrogel fibers: development and *in vitro* evaluation as a potential moist wound care dressing, *Int. J. Biol. Macromol.*, 2021, **168**, 601–610, DOI: 10.1016/j.ijbiomac.2020.12.088.

34 F. Azam, F. Ahmad and S. Ahmad, Preparation and Characterization of Alginate Hydrogel Fibers Reinforced by Cotton for Biomedical Applications, *Polymers*, 2022, **14**, 4707, DOI: 10.3390/polym14214707.

35 A. Kramar and J. González-benito, Preparation of cellulose acetate film with dual hydrophobic-hydrophilic properties using solution blow spinning, *Mater. Des.*, 2023, **227**, 111788, DOI: 10.1016/j.matdes.2023.111788.

36 S. Wu, X. Qin and M. Li, The structure and properties of cellulose acetate materials: a comparative study on electrospun membranes and casted films, *J. Ind. Text.*, 2014, **44**, 85–98, DOI: 10.1177/1528083713477443.

37 K. Y. Lee and D. J. Mooney, Alginate: properties and biomedical applications, *Prog. Polym. Sci.*, 2012, **37**, 106–126, DOI: 10.1016/j.progpolymsci.2011.06.003.

38 M. Z. A. Zulkifli, D. Nordin, N. Shaari and S. K. Kamadurin, Overview of Electrospinning for Tissue Engineering Applications, *Polymers*, 2023, **15**, 2418, DOI: 10.3390/polym15112418.

39 Y. B. Kim and G. H. Kim, PCL/Alginate Composite Scaffolds for Hard Tissue Engineering: Fabrication, Characterization, and Cellular Activities, *ACS Comb. Sci.*, 2015, **17**, 87–99, DOI: 10.1021/co500033h.

40 X. Dreux, C. Carrot, A. Argoud and C. Vergelati, Viscoelastic behaviour of cellulose acetate/triacetin blends by rheology in the melt state, *Carbohydr. Polym.*, 2019, **222**, 114973.

41 S. Phaiju, P. Mulmi, D. K. Shahi, T. I. Hwang, A. P. Tiwari, R. Joshi, H. R. Pant and M. K. Joshi, Antibacterial Cinnamon Essential Oil Incorporated Poly(ε-Caprolactone) Nanofibrous Mats: New Platform for Biomedical Application, *J. Inst. Sci. Technol.*, 2020, **25**, 9–16, DOI: 10.3126/jist.v25i2.33724.

42 M. E. Cuvelier and C. Berset, Use of a Free Radical Method to Evaluate Antioxidant Activity, *LWT - Food Sci. Technol.*, 1995, **28**, 25–30.

43 A. Akturk, Enrichment of Cellulose Acetate Nanofibrous Scaffolds with Retinyl Palmitate and Clove Essential Oil for Wound Healing Applications, *ACS Omega*, 2023, **8**, 5553–5560, DOI: 10.1021/acsomega.2c06881.

44 P. Wen, D. H. Zhu, H. Wu, M. H. Zong, Y. R. Jing and S. Y. Han, Encapsulation of cinnamon essential oil in electrospun nanofibrous film for active food packaging, *Food Control*, 2016, **59**, 366–376, DOI: 10.1016/j.foodcont.2015.06.005.

45 A. Li, I. N. Khan, I. U. Khan, A. M. Yousaf and Y. Shahzad, Gellan gum-based bilayer mucoadhesive films loaded with moxifloxacin hydrochloride and clove oil for possible treatment of periodontitis, *Drug Des., Dev. Ther.*, 2021, **15**, 3937–3952, DOI: 10.2147/DDDT.S328722.

46 M. Idrees, A. R. Mohammad, N. Karodia and A. Rahman, Multimodal Role of Amino Acids in Microbial Control and Drug Development, *Antibiotics*, 2020, **9**, 330, DOI: 10.3390/antibiotics9060330.

47 B. L. M. De Jonge, D. Gage and N. Xu, The Carboxyl Terminus of Peptidoglycan Stem Peptides Is a Determinant for Methicillin Resistance in *Staphylococcus aureus*, *Antimicrob. Agents Chemother.*, 2002, **46**, 3151–3155, DOI: 10.1128/AAC.46.10.3151.

48 D. Xu, Y. Li and T. Gu, D-Methionine as a biofilm dispersal signaling molecule enhanced tetrakis hydroxymethyl phosphonium sulfate mitigation of *Desulfovibrio vulgaris* biofilm and biocorrosion pitting, *Mater. Corros.*, 2014, **65**, 837–845, DOI: 10.1002/maco.201206894.

49 M. Cassone, P. Vogiatzi, R. La, V. De Olivier, P. Cudic, J. D. Wade and L. Otvos, Scope and limitations of the designer proline-rich antibacterial peptide dimer, A3-APO, alone or in synergy with conventional antibiotics, *Peptides*, 2008, **29**, 1878–1886, DOI: 10.1016/j.peptides.2008.07.016.

50 F. Rozgonyi, D. Szabo, B. Kocsis, E. Ostorházi, G. Abbadessa, M. Cassone, J. D. Wade and L. Otvos, The Antibacterial Effect of a Proline-Rich Antibacterial Peptide A3-APO, *Curr. Med. Chem.*, 2009, 3996–4002, DOI: 10.2174/092986709789352295.

51 E. T. Uyterhoeven, C. H. Butler, D. Ko and D. E. Elmore, Investigating the nucleic acid interactions and antimicrobial mechanism of buforin II, *FEBS Lett.*, 2008, **582**, 1715–1718, DOI: 10.1016/j.febslet.2008.04.036.

52 A. Tanhaeian, M. H. Sekhavati and M. Moghaddam, Antimicrobial activity of some plant essential oils and an antimicrobial – peptide against some clinically isolated pathogens, *Chem. Biol. Technol. Agric.*, 2020, 1–11, DOI: 10.1186/s40538-020-00181-9.

53 A. Zouhir, T. Jridi, A. Nefzi and J. Ben Hamida, Inhibition of methicillin-resistant *Staphylococcus aureus* (MRSA) by antimicrobial peptides (AMPs) and plant essential oils, *Pharm Biol.*, 2016, **54**, 3136–3150, DOI: 10.1080/13880209.2016.1190763.

54 Y. Xie and L. Yang, Calcium and Magnesium Ions Are Membrane-Active against Stationary-Phase *Staphylococcus aureus* with High Specificity, *Sci. Rep.*, 2016, **6**, 1–8, DOI: 10.1038/srep20628.

55 M. Ahmad, R. Kuldeep and G. Manabendra, Microbial biofilm: formation, architecture, antibiotic resistance, and control strategies, *Braz. J. Microbiol.*, 2021, 1701–1718, DOI: 10.1007/s42770-021-00624-x.

56 Z. Pang, R. Raudonis, B. R. Glick, T. Lin and Z. Cheng, Antibiotic resistance in *Pseudomonas aeruginosa*: mechanisms

and alternative therapeutic strategies, *Biotechnol. Adv.*, 2019, **37**, 177–192, DOI: **10.1016/j.biotechadv.2018.11.013**.

57 T. T. Ruckh and R. A. Oldinski, Antimicrobial effects of nanofiber poly(caprolactone) tissue scaffolds releasing rifampicin, *J. Mater. Sci.:Mater. Med.*, 2012, **23**, 1411–1420, DOI: **10.1007/s10856-012-4609-3**.

58 D. A. Pompa-Monroy, P. G. Figueroa-Marchant, S. G. Dastager, M. N. Thorat, A. L. Iglesias, V. Miranda-Soto, G. L. Pérez-González and L. J. Villarreal-Gómez, Bacterial biofilm formation using pcl/curcumin electrospun fibers and its potential use for biotechnological applications, *Materials*, 2020, **13**, 1–22, DOI: **10.3390/ma13235556**.

59 S. Lencova, M. Stindlova, K. Havlickova, V. Jencova, V. Peroutka, K. Navratilova, K. Zdenkova, H. Stiborova, S. Hauzerova, E. K. Kostakova, O. Jankovsky, P. Kejzlar, D. Lukas and K. Demnerova, Influence of Fiber Diameter of Polycaprolactone Nanofibrous Materials on Biofilm Formation and Retention of Bacterial Cells, *ACS Appl. Mater. Interfaces*, 2024, **16**, 25813–25824, DOI: **10.1021/acsami.4c03642**.

60 M. M. M. Kuypers, H. K. Marchant and B. Kartal, The microbial nitrogen-cycling network, *Nat. Rev. Microbiol.*, 2018, **16**, 263–276, DOI: **10.1038/nrmicro.2018.9**.

61 H. P. Kahyun, S. Dongjin, L. Minho and S. Chaenyung, Cellulose acetate nanoneedle array covered with phosphorylcholine moiety as a biocompatible and sustainable antifouling material, *Cellulose*, 2019, **26**, 8775–8788, DOI: **10.1007/s10570-019-02681-w**.

62 M. Sadekuzzaman, S. Yang, M. F. R. Mizan and S. D. Ha, Current and Recent Advanced Strategies for Combating Biofilms, *Compr. Rev. Food Sci. Food Saf.*, 2015, **14**, 491–509, DOI: **10.1111/1541-4337.12144**.

63 M. Denda, Keratinocytes at the uppermost layer of epidermis might act as sensors of atmospheric pressure change, *Extrem. Physiol. Med.*, 2016, **5**, 11–14, DOI: **10.1186/s13728-016-0052-2**.

64 A. Hoh and K. Maier, *Comparative Cytotoxicity Test with Human Keratinocytes, HaCaT Cells, and Skin Fibroblasts to Investigate Skin-Irritating Substances, Cell and Tissue Culture Models in Dermatological Research*, Springer, Berlin, Heidelberg, 1993, DOI: **10.1007/978-3-642-77817-9_38**.

65 H. P. Felgueiras, N. S. Murthy, S. D. Sommerfeld, M. M. Brás, V. Migonney and J. Kohn, Competitive Adsorption of Plasma Proteins Using a Quartz Crystal Microbalance, *ACS Appl. Mater. Interfaces*, 2016, **8**, 13207–13217, DOI: **10.1021/acsami.5b12600**.

66 W. W. Hu, Y. C. Wu and Z. C. Hu, The development of an alginate/polycaprolactone composite scaffold for *in situ* transfection application, *Carbohydr. Polym.*, 2018, **183**, 29–36, DOI: **10.1016/j.carbpol.2017.11.030**.

67 S. Chaiarwut, P. Ekabutr, P. Chuysinuan, T. Chanamuangkon and P. Supaphol, Surface immobilization of PCL electrospun nanofibers with pexiganan for wound dressing, *J. Polym. Res.*, 2021, **28**, 344, DOI: **10.1007/s10965-021-02669-w**.

68 C. Ahn, J.-H. Lee, M.-J. Park, J.-W. Kim, J. Yang, Y.-M. Yoo and E.-B. Jeung, Cytostatic effects of plant essential oils on human skin and lung cells, *Exp. Ther. Med.*, 2020, 2008–2018, DOI: **10.3892/etm.2020.8460**.

69 W. Prabhashini, K. Mendis, G. Arachchige and S. Premakumara, Anti – inflammatory, cytotoxicity and antilipidemic properties: novel bioactivities of true cinnamon (*Cinnamomum zeylanicum* Blume) leaf, *BMC Complementary Med. Ther.*, 2022, **5**, 1–15, DOI: **10.1186/s12906-022-03728-5**.

70 J. Guo, X. Jiang, Y. Tian, S. Yan, J. Liu, J. Xie, F. Zhang, C. Yao and E. Hao, Therapeutic Potential of Cinnamon Oil: Chemical Composition, Pharmacological Actions, and Applications, *Pharmaceuticals*, 2024, **17**, 1700, DOI: **10.3390/ph17121700**.

71 T. Petreus and B. Alexandru, Preparation and cytocompatibility evaluation for hydrosoluble phosphorous acid-derivatized cellulose as tissue engineering scaffold material, *J. Mater. Sci.:Mater. Med.*, 2014, **25**, 1115–1127, DOI: **10.1007/s10856-014-5146-z**.

72 W. Yuan, K. Wu, N. Liu, Y. Zhang and H. Wang, Cellulose acetate fibers with improved mechanical strength prepared with aqueous NMMO as solvent, *Cellulose*, 2018, **8**, DOI: **10.1007/s10570-018-2032-8**.

73 C. M. P. Ribeiro, J. Reece and J. W. Putney, Role of the cytoskeleton in calcium signaling in NIH 3T3 cells – An intact cytoskeleton is required for agonist-induced [Ca^{2+}](i) signaling, but not for capacitative calcium entry Role of the Cytoskeleton in Calcium Signaling in NIH 3T3 Cells, *J. Biol. Chem.*, 1997, **272**, 26555–26561, DOI: **10.1074/jbc.272.42.26555**.

74 A. M. Rahimi, M. Cai and S. Hoyer-fender, Heterogeneity of the NIH 3T3 Fibroblast Cell Line, *Cells*, 2022, **11**, 2677, DOI: **10.3390/cells11172677**.

75 M. Ben Amar, M. Wu and P. M. Curie-paris, Re-epithelialization: advancing epithelium frontier during wound healing, *J. R. Soc. Interface*, 2014, **11**, DOI: **10.1098/rsif.2013.1038**.

76 I. Pastar, O. Stojadinovic, N. C. Yin, H. Ramirez, A. G. Nusbaum, A. Sawaya, S. B. Patel, L. Khalid, R. R. Isseroff and M. Tomic-canic, Epithelialization in Wound Healing: A Comprehensive Review, *Adv. Wound Care*, 2014, **3**, 445–464, DOI: **10.1089/wound.2013.0473**.

77 E. Malikmammadov, T. E. Tanir, A. Kiziltay and V. Hasirci, PCL and PCL-Based Materials in Biomedical Applications, *J. Biomater. Sci., Polym. Ed.*, 2018, **29**, 863–893, DOI: **10.1080/09205063.2017.1394711**.

78 S. Yu, Y. Gao, X. Mei, T. Ren, S. Liang, Z. Mao and C. Gao, Preparation of Arg-Glu-Asp-Val peptide density gradient on hyaluronic acid-coated poly(#-caprolactone) film and its influence on the selective adhesion and directional migration of endothelial cells, *ACS Appl. Mater. Interfaces*, 2016, **8**, 29280–29288, DOI: **10.1021/acsami.6b09375**.

79 R. In, J. M. Kemppainen, D. Ph, M. T. Harris, S. J. Hollister and D. Ph, Effect of Polycaprolactone Scaffold Permeability, *Tissue Eng. Part A*, 2011, **17**, 1831–1839, DOI: **10.1089/ten.tea.2010.0560**.

80 S. Kamalipooya, S. Fahimirad, H. Abtahi, M. Golmohammadi, M. Satari, M. Dadashpour and D. Nasrabadi, Diabetic

wound healing function of PCL/cellulose acetate nanofiber engineered with chitosan/cerium oxide nanoparticles, *Int. J. Pharm.*, 2024, **653**, 123880, DOI: **10.1016/J.IJPHARM.2024.123880**.

81 M. Arumugam, B. Murugesan, D. Kumar Chinnalagu, Y. Cai, S. Ponnurengam Malliappan, P. Balasekar, G. Rengasamy, K. Chinniah and S. Mahalingam, Multifunctional silk fibroin and cellulose acetate composite nanofibers incorporated with palladium and platinum nanoparticles for enhanced wound healing: comprehensive characterization and in vivo assessment, *Colloids Surf., A*, 2024, **684**, 133153, DOI: **10.1016/J.COLSURFA.2024.133153**.

82 M. Zhang and X. Zhao, International Journal of Biological Macromolecules Alginate hydrogel dressings for advanced wound management, *Int. J. Biol. Macromol.*, 2020, **162**, 1414–1428, DOI: **10.1016/j.ijbiomac.2020.07.311**.

83 J. Koehler, L. Wallmeyer, S. Hedtrich, A. M. Goepferich and F. P. Brandl, pH-Modulating Poly(ethylene glycol)/Alginate Hydrogel Dressings for the Treatment of Chronic Wounds, *Macromol. Biosci.*, 2017, **17**, 1–11, DOI: **10.1002/mabi.201600369**.

84 J. Zhang, A. Zhang and Y. Song, Wound healing mechanism of antimicrobial peptide cathelicidin-DM, *Front. Bioeng. Biotechnol.*, 2022, **10**, 977159, DOI: **10.3389/fbioe.2022.977159**.

85 C. Physiology, The Designer Antimicrobial Peptide A-hBD-2 Facilitates Skin Wound Healing by Stimulating Keratinocyte Migration and Proliferation, *Cell. Physiol. Biochem.*, 2018, **51**, 647–663, DOI: **10.1159/000495320**.

86 A. Daemi, M. Lotfi, M. R. Farahpour, A. Oryan, J. Ghayour and A. Sonboli, Topical application of Cinnamomum hydroethanolic extract improves wound healing by enhancing re-epithelialization and keratin biosynthesis in streptozotocin-induced diabetic mice Topical application of Cinnamomum hydroethanolic extract improves wound heal, *Pharm. Biol.*, 2019, **57**, 799–806, DOI: **10.1080/13880209.2019.1687525**.